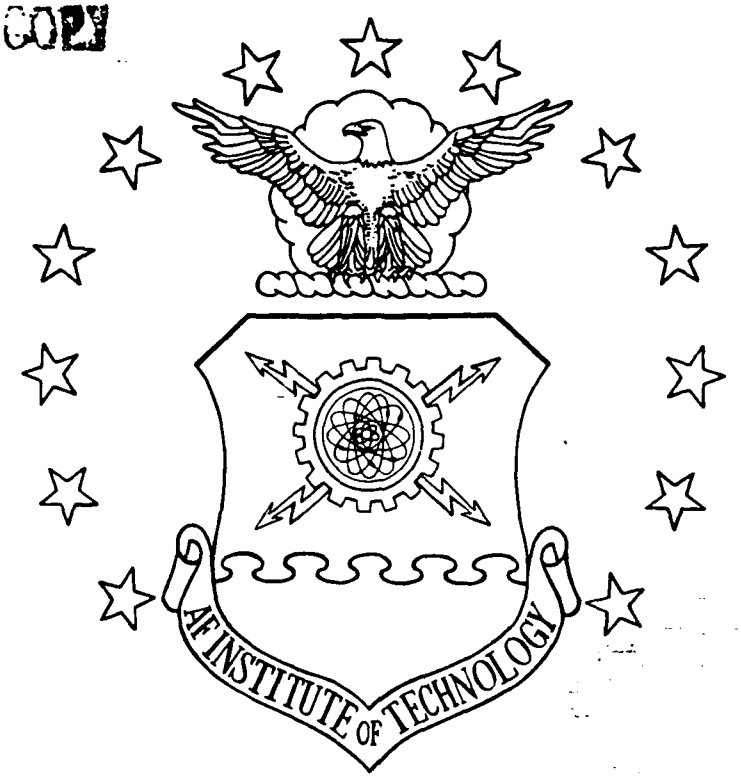

AN ITERATIVE SOLUTION TO AEROELASTIC EFFECTS IN POTENTIAL FLOW

THESIS

Raymond C. Maple
Captain, USAF

AFIT/GAE/ENY/89D-22

DEPARTMENT OF THE AIR FORCE
AIR UNIVERSITY
AIR FORCE INSTITUTE OF TECHNOLOGY

Wright-Patterson Air Force Base, Ohio

AFIT/GAE/ENY/89D-22

AN ITERATIVE SOLUTION TO AEROELASTIC EFFECTS IN POTENTIAL FLOW

THESIS

Presented to the Faculty of the School of Engineering
of the Air Force Institute of Technology
Air University
In Partial Fulfillment of the
Requirements for the Degree of
Master of Science in Aeronautical Engineering

Raymond C. Maple, B.S.
Captain, USAF

December 1989

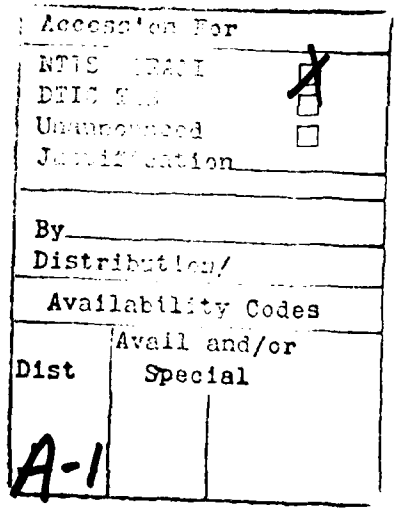

Approved for public release; distribution unlimited

Preface

The purpose of study was to develop a means of incorporating aeroelastic effects into a three dimensional unsteady potential flow solution. As a step towards the inclusion of unsteady aeroelastic effects, a static development was performed.

Extensive modifications were made to an existing three dimensional vortex paneling FORTRAN code to allow it to be used iteratively with MSC/NASTRAN to achieve aeroelastic equilibrium for arbitrary bodies. Much attention was given to the development of a flexible interface and to improving the efficiency of the paneling code. The iterative method was evaluated, but lack of sufficient computational facilities prevented complete testing of the implementation. This work should be continued and expanded, as it represents a significant enhancement to the modeling capabilities of the potential flow.

I would like to thank my thesis advisor, Capt. Curtis P. Mracek, whose continued help and support through all the difficult and frustrating times made this thesis possible. I would also like to thank Dr. A. Palazatto and Capt. H. Gans for their help with the finite element modeling and use of MSC/Nastran. Finally, I would like to thank my wife Jane-Anne and my daughter Sarah for their love and support during the preparation of this thesis.

Raymond C. Maple

Table of Contents

List of Figures

List of Tables

Abstract

The purpose of the study was to develop a method of incorporating static aeroelastic effects into a vortex paneling aerodynamic solution. The study had two basic objectives: (1) Devise a solution technique; (2) Implement the technique and analyze several test cases.

An iterative solution is developed which uses MSC/NASTRAN to perform structural analysis, and a three-dimensional vortex paneling method to perform aerodynamic analysis. The theory behind the method and details of the implementation are presented.

The method is tested for three bodies: a unit aspect ratio rectangular flat plate wing, a rectangular flat plate wing with aspect ratio 6, and a hollow sphere. Results of these tests are used to evaluate both the general performance of the implementation, and the performance for the specific tests. The results indicate that the iterative solution method is robust and could potentially be used for solving a variety of aeroelastic problems. Recommendations for further development, evaluation, and use are made.

AN ITERATIVE SOLUTION TO AEROELASTIC EFFECTS IN POTENTIAL FLOW

I. INTRODUCTION

Problem Statement

Develop a means of incorporating aeroelastic effects into an existing unsteady potential flow numerical solution.

Scope of Development

As a first step in the resolution of the stated problem, this study focuses on development for steady state cases. Particular attention is paid to improving the efficiency of the potential flow solution and providing it with a flexible interface which will serve as the foundation for future work.

Method of Approach

The method developed solves for the steady state solution to the aeroelastic problem by the alternate use of a three-dimensional potential flow code and a general purpose structural finite element code. Results from the two codes are used iteratively until equilibrium between structural and aerodynamic forces is achieved.

Background and Research

In a time when prototype aircraft can cost hundreds of millions of dollars, it becomes imperative that designs be tested as thoroughly and accurately as possible before any

hardware is built. This has led to increased reliance on computer simulation of systems. Simulations require accurate modeling, and much effort has gone into devising accurate modeling techniques for all aspects of flight, including aerodynamic and aeroelastic phenomena.

Aeroelasticity. The importance of aeroelasticity in the design of aircraft was recognized in the 1920's, but it was not until the late 30's and 40's that serious consideration was given tc aeroelastic phenomena. During this time period, aircraft designs began incorporating thin, high aspect ratio lifting surfaces which were inherently less rigid than earlier designs. In the late 1940's, as fighter aircraft began operating at high subsonic speeds with correspondingly high dynamic pressures, the incorporation of aeroelasticity in fighter design became essential. (17:1.1)

Early aeroelastic analysis was limited to static and quasi-static cases. The effects of static aeroelasticity on aircraft performance can be divided into three categories: divergence, control effectiveness, and static stability. (18:2)

Divergence occurs when aerodynamic moments exceed the torsional strength of a wing and structural failure occurs. Divergence is usually associated with a particular dynamic pressure, $\bar{q}_D$, and all aircraft are designed to fly below the corresponding divergence velocity. (4:6)

Control effectiveness is affected by static aeroelasticity in several ways. In a technical report prepared for the Air Force in 1957, the J.B. Rea Company identifies two prime examples. Consider first the wing section in Figure 1. The deflected control surface creates a moment about the elastic axis of the wing, causing the wing to twist nose down, decreasing or even reversing the effect of the control input.(18:8) A second effect involves fuselage bending. A long, relatively flexible fuselage such as that of the B-52 can bend significantly, changing the angle of attack of horizontal and vertical tail surfaces.(18:15)

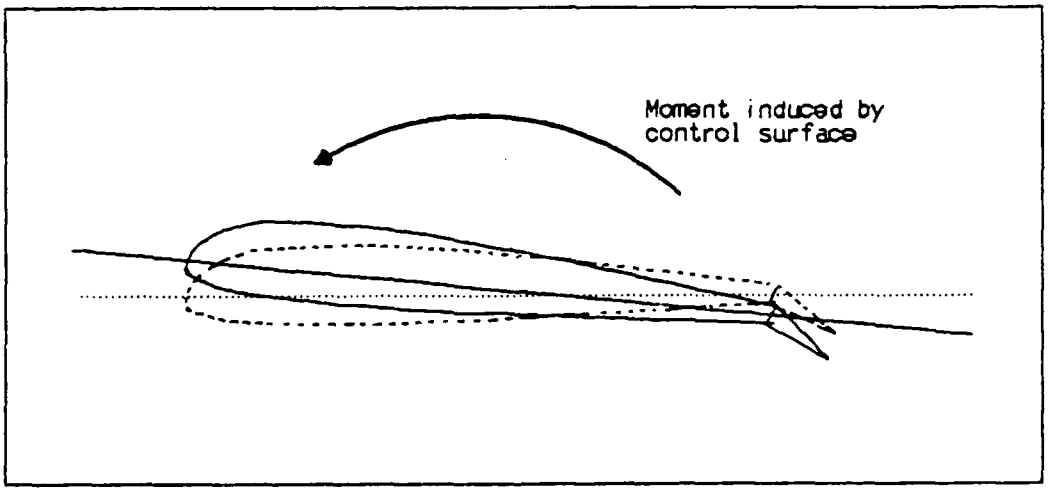

Figure 1. Impact of Aeroelastic Twist on Control Effectiveness.

Perhaps the most significant effect of static aeroelasticity on subsonic aircraft is that of modifying stability derivatives. William P. Rodden describes the significance of wing bending.

> The dihedral effect can be a critical aeroelastic problem because of the importance of dihedral in determining dynamic stability in the spiral and Dutch roll modes of motion and the large changes in dihedral that result from symmetrical wing bending during longitudinal maneuvers that approach limit load factor.(11:368)

Lift and drag are also affected by wing bending and torsion.

As aircraft speeds moved into the supersonic region, flutter, a dynamic aeroelastic effect, became a serious problem. A large percentage of recent aeroelastic study has been devoted to the study of flutter. Static aeroelastic effects, however, are still recognized as important design considerations. The thin airfoils and high load factors of supersonic fighter aircraft can lead to significant elastic effects on stability derivatives.(15:2-2,2-3)

With the introduction of composite wing structures, the ability to utilize static aeroelastic effects is possible. This design technique is called aeroelastic tailoring. Aeroelastic tailoring is

> ... a design technique in which directional stiffness is used in aircraft structural design to control aeroelastic deformation, static or dynamic, in such a way that the aerodynamic and structural performance is affected in a beneficial way. (15:2-4)

Aeroelastic tailoring can be used to increase control effectiveness, decrease drag, and help control flutter and divergence while using a lighter structure.(16:2)

Formulation and Solution of the Aeroelastic Equations. Early formulations of the aeroelastic problem centered on the typical section developed by Theodorsen and Garrick, which is an attempt to model the elastic behavior of a wing

at a particular location along the span. (1:189) Other formulations include one-dimensional and two-dimensional analyses. Current finite element approaches allow the investigation of general three-dimensional structures. The development presented here makes use of a three dimensional potential flow aerodynamic code and a general purpose finite element structural code in an iterative scheme.

The iterative scheme used in this development is not new. It is described in Reference 18, published in 1957. The primary difference between the effectiveness of the method in 1957 and the effectiveness today is the ability to calculate, with the aid of computers, aerodynamic loads and structural deflections for arbitrary shapes with reasonably high accuracy.

The aerodynamic code used in this work was developed by Mracek (8). It consists of a three-dimensional vortex paneling method which possesses many features not seen in previous works. Among these are simplified modeling and the ability to predict general unsteady motion with progressive wake modeling. For a complete description of this work and a comprehensive bibliography of prior developments leading to it, see Reference 8.

Structural analysis is performed using the well known general purpose finite element code, MSC/NASTRAN, developed by the MacNeal-Schwendler Corp. Version 66 was used for this work. Reference 14 provides an excellent overview of

the portions of this finite element package which pertain to this study.

Assumptions

It is assumed in this work that structural displacements due to aerodynamic loads are small. This assumption is required both by the linear displacement finite element method, and by the method of iteration used to attain aeroelastic equilibrium.

Test Cases

Analysis is performed for three bodies. A flat rectangular wing with an aspect ratio of six is compared to one-dimensional aeroelastic theory. Next, a flat rectangular wing with unit aspect ratio is analyzed at various angles of attack, focusing on qualitative changes in induced moments and forces. Finally, the ability of the method to handle non-lifting shell structures is shown through the analysis of a spherical shell.

II. THEORY

Introduction

The theoretical foundation upon which this work is built can be divided into four primary groups. First there is aeroelastic theory, which provides the equations of motion. A means of solving these equations is then needed. In this study, the equations are solved by dividing the aeroelastic problem into its two components, aerodynamics and structural analysis, which in turn have their own theoretical bases. This chapter follows this breakdown. In the first part of the chapter, the steady state one-dimensional aeroelastic equations of motion are derived. Next, the iterative technique for solving these equations is developed. Finally, the aerodynamic and structural components of the iteration are discussed.

Static One Dimensional Aeroelasticity

Traditionally, static aeroelasticity is introduced in one of two ways. The first is by means of the typical section (1:189-279), which does not model an actual wing but serves to illustrate the fundamental concepts of static aeroelasticity. The second, more realistic, formulation models a wing as a bending-torsion beam whose behavior can be described by just one variable. This discussion will use the latter.

While the iterative solution developed in the next section is not based on a direct solution of the equations of static aeroelasticity, a review of the classical one dimensional solution gives some insight into the problem and serves as a baseline for evaluation of results. In this section, the static torsional equation of motion is derived for a flat plate wing. (Figure 2.) An expression for the vertical displacement at the wing tips is then developed. The derivation that follows is from Dowell (4:15-18).

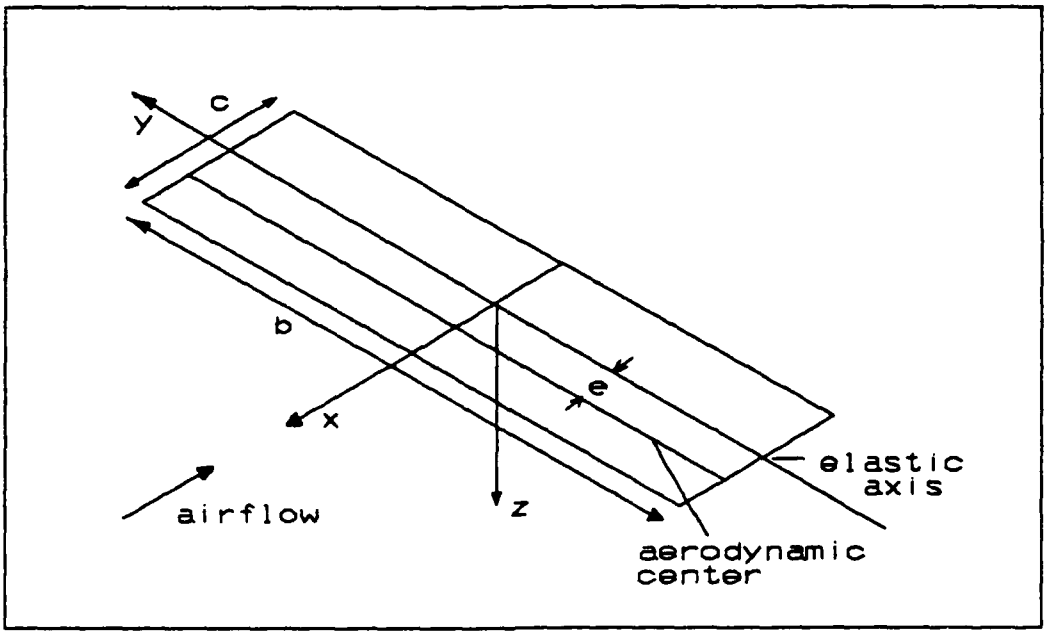

Figure 2. Flat Plate Rectangular Wing

The torsional equation of motion is found by equating the external (aerodynamic) and internal moments acting on the wing. Summing the moments acting on a differential strip of the wing (Figure 3), the equilibrium condition is found to be

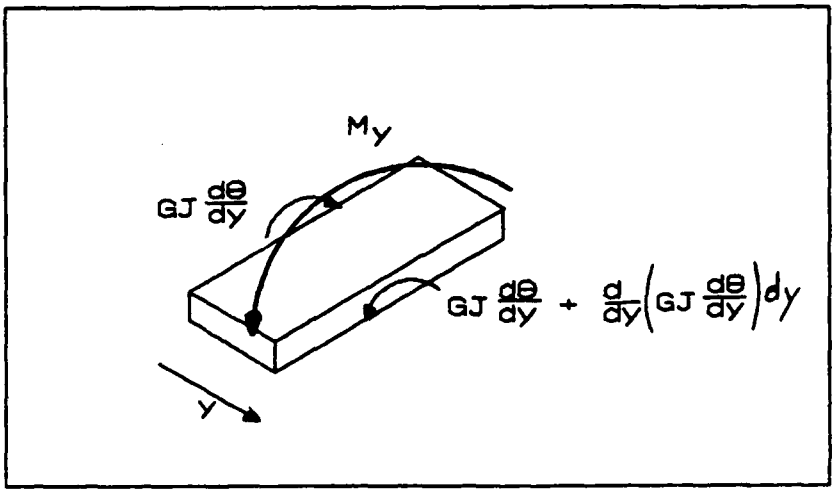

Figure 3. Moments on a Differential Strip of Wing

$$\frac{d}{dy}\left(GJ\frac{d\theta}{dy} \right) + M_y = 0 \qquad (2.1)$$

where GJ is the torsional stiffness of the plate and My is the applied (aerodynamic) moment per unit span. Assuming that the center of the wing is fixed and the tips free, the boundary conditions are

$$\theta = 0 \text{ at } y = 0$$

$$GJ\frac{d\theta}{dy} = 0 \text{ at } y = \pm\ell \qquad (2.2)$$

where ℓ is the semispan (b/2) of the wing.

The aerodynamic moment per unit span is

$$M_y = M_{ac} + eL \qquad (2.3)$$

M_{ac} being the moment about the aerodynamic center, L the lift per unit length and e the distance between the aerodynamic center and the elastic axis. From aerodynamic theory, M_{ac} is

$$M_{AC} = \bar{q}c^2 C_{M_{ac}} \tag{2.4}$$

and for simplicity, the lift distribution is assumed to be

$$L(y) = \bar{q}cC_L = \bar{q}c\ C_{L_\alpha}\left(\alpha_o + \theta(y)\right) \tag{2.5}$$

where

$$C_{L_\alpha} = \frac{dC_L}{d\alpha} \tag{2.6}$$

and $\bar{q}$ is the dynamic pressure, c the wing chord, and α_o the undeformed angle of attack.

Nondimensionalizing equation 2.1 results in

$$\frac{d^2\theta}{d\tilde{y}^2} + \lambda^2\theta = K \tag{2.7}$$

where

$$\tilde{y} = \frac{y}{\ell} \tag{2.8}$$

$$\lambda^2 = \frac{\bar{q}\ell^2}{GJ}\, c\ C_{L_\alpha} e \tag{2.9}$$

$$K = -\frac{\bar{q}c\ell^2}{GJ}\left(e\ C_{L_\alpha}\ \alpha_o + c\ C_{M_{ac}}\right) \tag{2.10}$$

with the boundary conditions becoming

$$\theta = 0 \text{ at } \tilde{y} = 0$$

$$GJ\frac{d\theta}{d\tilde{y}} = 0 \text{ at } \tilde{y} = \pm 1 \tag{2.11}$$

The general solution to Equation 2.7 is

$$\theta = A \sin(\lambda\tilde{y}) + B \cos(\lambda\tilde{y}) + \frac{K}{\lambda^2} \tag{2.12}$$

Applying boundary conditions and solving for the unknowns yields

$$\theta = \frac{K}{\lambda^2}\left(1 - \tan(\lambda) \sin(\lambda\tilde{y}) - \cos(\lambda\tilde{y})\right) \tag{2.13}$$

The static aeroelastic stability of a wing is a function of the dynamic pressure. The divergence dynamic pressure $\bar{q}_D$ is found by using Equations 2.13 and 2.9 and letting θ go to infinity. Solving for $\bar{q}_D$ results in

$$\bar{q}_D = \frac{\pi^2 GJ}{8\,\ell^2 ce C_{L_\alpha}} \tag{2.14}$$

For a flat plate wing some simplifications may be made to the above equations. If h is the thickness of the plate and h << c, then

$$J = \frac{ch^3}{3} \tag{2.15}$$

The elastic axis for a uniform rectangular plate lies along the center of the chord, while the aerodynamic center is 1/4 chord from the leading edge. The distance from the

elastic axis to the aerodynamic center is therefore c/4. In addition, for a flat plate, $C_{M_{ac}} = 0$ for all angles of attack. Making these substitutions leads to

$$K = -\frac{3}{4}\frac{\bar{q}c\ell^2}{Gh^3} C_{L_\alpha} \alpha_o \tag{2.16}$$

$$\lambda^2 = \frac{3}{4}\frac{\bar{q}c\ell^2}{Gh^3} C_{L_\alpha} \tag{2.17}$$

$$\theta = -\alpha_o \left(1 - \tan(\lambda) \sin(\lambda\tilde{y}) - \cos(\lambda\tilde{y})\right) \tag{2.18}$$

Knowing the angle of attack at all locations along the span, one can now derive an expression for the vertical displacement at the tips. The equation of motion for a pure bending beam is:

$$EI \frac{d^4w}{d\tilde{y}^4} = f(\tilde{y}) \tag{2.19}$$

where EI is the beam bending stiffness, w is the vertical displacement, and $f(\tilde{y})$ is the normal load as a function of $\tilde{y}$.(5:92) The function $f(\tilde{y})$ is aproximated by

$$f(\tilde{y}) = -\frac{\ell^4 L(\tilde{y})}{\cos(\alpha_o)} = -\frac{\ell^4 \bar{q}c}{\cos(\alpha_o)} C_{L_\alpha}\left(\alpha_o + \theta\right) \tag{2.20}$$

Substituting Equations 2.18 and 2.20 into Equation 2.19 yields

$$EI \frac{d^4w}{d\tilde{y}^4} = \frac{q\bar{c}\ell^4}{\cos(\alpha_o)} * C_{L_\alpha} \alpha_o \left(\tan(\lambda) \sin(\lambda\tilde{y}) - \cos(\lambda\tilde{y})\right) \tag{2.21}$$

Boundary conditions for the wing are the same as those for a cantelevered beam, specifically

$$w(0) = 0 \qquad \left.\frac{dw}{d\tilde{y}}\right|_{\tilde{y}=0} = 0$$

$$EI \left.\frac{d^2w}{d\tilde{y}^2}\right|_{\tilde{y}=\pm l} = 0 \qquad EI \left.\frac{d^3w}{d\tilde{y}^3}\right|_{\tilde{y}=\pm l} = 0 \tag{2.22}$$

Successive integration and application of the boundary conditions yields

$$w(\tilde{y}) = -\frac{\bar{q}c\ell^4}{EI\ \cos(\alpha_o)}\, C_{L_\alpha}\alpha_o * \left[\frac{1}{\lambda^4}\left(\tan(\lambda)\ \sin(\lambda\tilde{y}) - \cos(\lambda\tilde{y})\right) + \frac{1}{\lambda^2}\frac{\tilde{y}^2}{2\ \cos(\lambda)} - \frac{1}{\lambda^3}\tan(\lambda)\tilde{y} - \frac{1}{\lambda^4}\right] \tag{2.23}$$

Recognizing that the wing is a plate and that Poisson effects will be significant, the beam bending stiffness, EI, is modified by including a correction term, $1-\nu^2$. This term appears in the definition of flexural rigidity from fourth order plate theory, the analog of beam bending stiffness. Substituting for the inertia term, the modified bending stiffness becomes

$$\frac{EI}{\left(1 - \nu^2\right)} = \frac{Ech^3}{12\left(1 - \nu^2\right)} \tag{2.24}$$

With this substitution, the displacement at the tips ($y = \pm\ell$) becomes

$$w(1) = -\frac{12\bar{q}\ell^4\left(1-\nu^2\right)}{Eh^3\cos(\alpha_o)} C_{L_\alpha}\alpha_o \left[\frac{1}{\lambda^4}\frac{1}{\cos(\lambda)}\right.$$

$$\left. + \frac{1}{\lambda^2}\frac{1}{2\cos(\lambda)} - \frac{1}{\lambda^3}\tan(\lambda) - \frac{1}{\lambda^4}\right] \qquad (2.25)$$

Equations 2.18 and 2.25 represent a closed form solution for the twist and deflection of a wing due to aerodynamic loads. They were, however, developed subject to several simplifying assumptions. In the next section, a more general method of solving the static aeroelastic problem is developed.

An Iterative Solution

The aeroelastic equations of motion, whether one-dimensional or three-dimensional, are merely statements of equilibrium between internal structural forces and external aerodynamic forces. The method developed here is a simple iterative technique for reaching the point of equilibrium between internal and external loads. Used in the iteration are a three dimensional potential flow code and a general purpose structural finite element analysis.

The process is begun by calculating the aerodynamic loads induced on an undeformed body. These loads are used by the finite element code to deform the body. When the deformed body is placed in the potential flow, a new set of aerodynamic loads are generated, which are in turn applied to the (undeformed) body. The load generation - deformation

cycle is repeated until both the load and the deformation do not change from one iteration to the next. This process is represented graphically in Figure 4.

In theory, the iteration stops when the loads imposed on the body equal those required to deform the body. In practice this is true only to the extent that the model being analyzed is reaching an equilibrium point when the external (aerodynamic) loads are applied to the undeformed body. The errors incurred by this limitation are small provided displacments are small.

The small displacement assumption is utilized in several aspects of the iterative process. Linear displacement finite element theory requires small displacements. Linear finite element theory also assumes that applied loads remain constant in magnitude and direction as the body deforms, which is the source of the discrepancy between aerodynamic loads and internal stresses when the iterative process halts.

In reality, the problem is non-linear in nature. As a body subjected to aerodynamic loads deforms, both the magnitude and the direction of the applied load changes. The direction changes because a pressure force always acts normal to a surface. The magnitude changes for two reasons. First, as the shape of the body changes, the pressures in the flow change. This is the major source of change in load magnitude and is accounted for in the present method. The

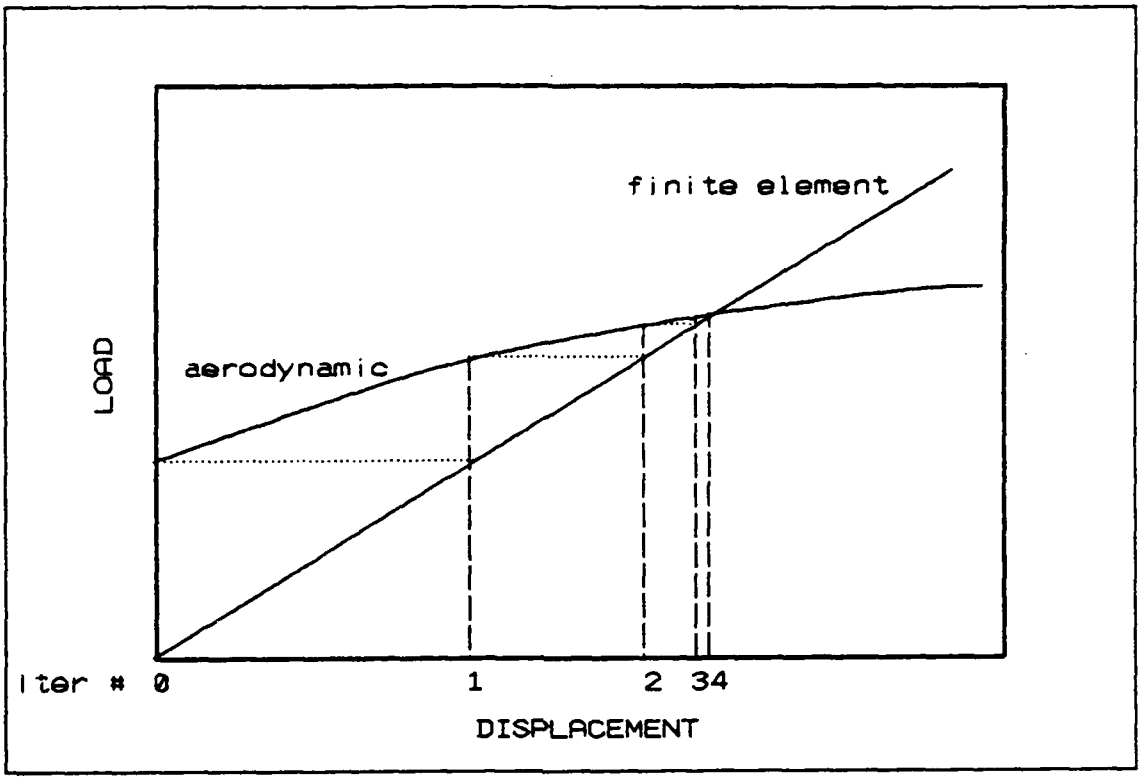

Figure 4. Graphical Representation of the Iterative Process

second change in magnitude comes about because as the body deforms, the area over which external pressures act changes. This change is not accounted for in the present method.

When displacements are small, changes in the surface area and normal direction are small, and load variations due to pressure changes in the flow dominate.

It is observed that these errors could have been eliminated by applying loads to the body (deformed or undeformed) which produced them. This requires that element strain energies from the previous iteration be provided as input to the finite element solution. To accomplish this

with MSC/NASTRAN, one must input temperature gradients which cause thermal strains equal to the desired strains. Calculation of these "temperatures" is not straightforward. Because of the difficulties in making the "temperature" calculations and the magnitude of the errors involved, no attempt at this form of iteration was made.

In the next two sections the aerodynamic and structural components of the iterative process are discussed.

The Potential Flow Solution

The field equations for incompressible potential flow are:

- incompressibility

$$\text{div}(\overline{V}) = \nabla^2\phi = 0 \tag{2.26}$$

- equation of motion

$$\frac{\delta\phi}{\delta t} + \frac{1}{2}\Big(\text{grad } \phi \Big)^2 + \frac{P}{\rho} - \overline{U} = f(t) \tag{2.27}$$

where ϕ is the velocity potential function, $\overline{V} = \nabla\phi$, and $\overline{U}$ is the scalar potential function for a body force. (6:245) Equation 2.26 is a statement of the divergenceless condition and Equation 2.27 is the unsteady Bernoulli equation. When a body is placed in the flow, the total velocity $\overline{V}$, may be written as

$$\overline{V} = \overline{V}_\infty + \overline{V}_d \tag{2.28}$$

where $\overline{V}_\infty$ is the free stream velocity and $\overline{V}_d$ is a

superimposed disturbance velocity caused by the body. Boundary conditions are then (6:249)

$$\bar{V} \cdot \hat{n} = 0 \quad \text{at the surface}$$
$$\bar{V}_d = 0 \quad \text{at infinity} \tag{2.29}$$

Equations 2.29 state that no flow may pass through the body, and that the body must have no effect on the flow at infinity.

When the body placed in the flow is a thin lifting surface, two additional conditions must be met. They are the conservation of circulation in the wake (6:242) and the Kutta condition. (6:392,393)

$$\frac{D\Gamma}{Dt} = 0 \quad \text{on the wake} \tag{2.30}$$

$$\Delta C_p = 0 \quad \text{along the trailing edge} \tag{2.31}$$

The paneling method developed by Mracek models the body in the flow as a collection of triangular vortex sheets, the corners of which lie on the body. The vorticity distribution in the panel is a linear function of the vorticity at the corners (nodes). The wake is modeled as a lattice of constant strength vortex cores. For a complete derivation of the modeling technique see Reference 8.

Flow induced by a vorticity distribution satisfies the divergenceless condition provided the vorticity distribution, $\bar{\gamma}$, is itself divergenceless, i.e.

$$\text{div}(\bar{\gamma}) = 0 \tag{2.32}$$

For an assembly of triangles, this condition may be written as

$$D\,\bar{\Omega} = \bar{0} \tag{2.33}$$

where D ($m \times n$, $n > m$)is a matrix of coefficients relating the divergence of the vorticity distributions on the triangles to the vorticity at the nodes, and $\bar{\Omega}$ is the vector of nodal vorticities.

The no penetration condition is satisfied at control points located at the centroid of each triangle. For the assembled triangles, the matrix equation to be satisfied is

$$A\,\bar{\Omega} = \bar{U} \tag{2.34}$$

where A ($m \times n$) are influence coefficients which relate the normal velocity at the control point to nodal vorticities, $\bar{\Omega}$ is again the vector of nodal vorticities, and $\bar{U}$ is a vector of inertial velocities at the control points.

Equation 2.34 must be solved subject to the constraints in Equation 2.33. The solution technique originally used by Mracek, concatenation of the matrices and solution via a weighted least squares method (8:29), has many drawbacks. The divergenceless conditions are not solved exactly, and the method involves repeatedly solving large matrix equations.

An improved solution technique was devised. It is clear that the matrices A and D are linear transforms from R_n to R_m, and that the divergenceless conditions require that the vector $\bar{\Omega}$ lie in the null space of D. From linear algebra, a basis for the null space of D may be obtained from the row-echelon form of D. (9:158) The constraint equations may be rearranged such that the row-echelon form of D is

$$\begin{bmatrix} I_k & B \\ 0 & 0 \end{bmatrix} \tag{2.35}$$

where B is k x (n-k) k being rank(B). The following equation is then equivalent to Equation 2.33.

$$\begin{bmatrix} I_k & B \\ 0 & 0 \end{bmatrix} \begin{Bmatrix} \bar{\omega}_1 \\ \bar{\omega}_2 \end{Bmatrix} = \begin{Bmatrix} \bar{0} \\ \bar{0} \end{Bmatrix} \tag{2.36}$$

where $\bar{\omega}_1$ is k x 1 and $\bar{\omega}_2$ is (n-k) x 1. The solution to this equation is

$$\bar{\omega}_1 = -B\bar{\omega}_2 \tag{2.37}$$

or

$$\bar{\Omega} = \begin{bmatrix} -B \\ I_{n-k} \end{bmatrix} \bar{\omega}_2 = D_{re}\bar{\omega}_2 \tag{2.38}$$

Substituting this result into Equation 2.34, one gets

$$A\, D_{re}\bar{\omega}_2 = \bar{U} \tag{2.39}$$

The least squares solution for $\bar{\omega}_2$ is obtained by solving

$$D_{re}^{T} A^{T} A \, D_{re} \bar{\omega}_2 = D_{re}^{T} A^{T} \bar{U} \qquad (2.40)$$

The vector $\bar{\Omega}$ obtained by substituting the result of Equation 2.40 into Equation 2.38 satisfies the divergenceless equations exactly, and represents the point in the null space of D that is closest, in a least squares sense, to the true solution of Equation 2.34. The resulting error in the no penetration condition is given by

$$\bar{e} = \bar{U} - A \bar{\Omega} \qquad (2.41)$$

Besides having the divergenceless conditions satisfied exactly, this method of solution has the advantage of requiring the solution of a smaller set of simultaneous equations. The matrix D_{re} need only be calculated once per iteration, but Equation 2.40 is typically solved up to 60 times per iteration. The savings in computational time can be very significant.

Because the no penetration conditions are not satisfied exactly, some modeling sensitivity is built into the solution. It is possible to have a model for which the errors are too large, making the model unusable. (see Chapter III.) .

Nodal Pressures. The function the aerodynamic solution in the iterative method is to calculate pressure loads on the body. In the present method, only the pressure values at the nodes are required.

For static steady state conditions, Equation 2.27 reduces to the steady Bernoulli's equation.

$$\frac{1}{2} V^2 + \frac{p}{\rho} = \text{const} \tag{2.42}$$

The conditions close to the body are thus related to the free stream conditions.

$$\frac{1}{2} V_\infty^2 + \frac{p_\infty}{\rho_\infty} = \frac{1}{2} V^2 + \frac{p}{\rho} \tag{2.43}$$

$$\frac{p - p_\infty}{\rho} = \frac{V^2 - V_\infty^2}{2} \tag{2.44}$$

The nondimensional pressure coefficient is defined as (6:500)

$$C_p = \frac{p - p_\infty}{\frac{1}{2}\rho V_\infty^2} \tag{2.45}$$

Substituting Equation 2.44 into Equation 2.45 gives

$$C_p = 1 - \left(\frac{V}{V_\infty} \right)^2 \tag{2.46}$$

Therefore, to find the pressure at the node, one only has to find the velocity at the node.

The velocity induced above and below a vorticity distribution may be expressed as

$$\bar{V}_u = \bar{V}_m + \frac{1}{2} \Delta\bar{V} \tag{2.47}$$

$$\bar{V}_l = \bar{V}_m + \frac{1}{2} \Delta\bar{V} \tag{2.48}$$

where $\bar{V}_u$ is the velocity above the distribution, $\bar{V}_l$ the velocity below, $\bar{V}_m$ the velocity between the upper and lower surfaces, and $\Delta\bar{V}$ the velocity jump from upper to lower surfaces. $\Delta\bar{V}$ is related to the vorticity distribution by (8:49)

$$\Delta\bar{V} = \bar{\gamma} \times \hat{n} \tag{2.49}$$

where $\hat{n}$ is the unit normal to the surface. At the node, the vorticity $\bar{\Omega}_n$ is perpendicular to the surface normal and Equation 2.49 reduces to

$$|\Delta\bar{V}| = |\bar{\Omega}_n| \tag{2.50}$$

For a closed body, $\bar{V}_l$, the velocity within the body, is zero. Solving Equation 2.48 for $\bar{V}_m$ and using Equations 2.47 and 2.50, the velocity at the node is found to be

$$|\bar{V}| = |\bar{\Omega}| \tag{2.51}$$

and the pressure coefficient is

$$C_p = 1 - \left(\frac{\Omega_n}{V_\infty} \right)^2 \tag{2.52}$$

For a thin lifting surface, $\bar{V}_l$ is not zero. The steady nondimentional pressure differential between the upper and lower surfaces is

$$\Delta C_p = C_{p_l} - C_{p_u} = \frac{p_l - p_u}{\frac{1}{2}\rho V_\infty^2} \tag{2.53}$$

Substituting Equation 2.44 into 2.53 one gets

$$\Delta C_p = \frac{1}{V_\infty^2} \left(V_u^2 - V_l^2 \right) \qquad (2.54)$$

Using the relationships in Equations 2.47, 2.48, 2.50, and simplifying, Equation 2.54 reduces to

$$\Delta C_p = 2 \left(\frac{1}{V_\infty^2} \bar{V}_m \cdot \nabla \bar{V} \right) \qquad (2.55)$$

Numerically, the mean velocity vector $\bar{V}_m$ is found by calculating the velocity at the node induced by all the vortex triangles and the wake vortex cores.

The Finite Element Analysis

Finite element analysis is used in this work to determine the translational displacements of the node points. The underlying theory of the method used was developed over twenty years ago and is well published. For this reason, a theoretical discussion of finite element techniques is not included in this work. What follows is a discussion of the properties of the element used in this analysis, and the rationale behind the choice of that element. For a review of finite element methods see Cook. (Reference 3.)

The element used for both the sphere and flat plate analyses is the CTRIA3 element provided within MSC/NASTRAN. This is a flat, three noded element with combined bending

and membrane effects.(10:2.4-118) The decision to use this particular element was driven by two considerations.

The first was data compatability with the potential flow solution. Geometrically, the data required for the CTRIA3 element is identical to that which describes the vortex panels in the potential flow. This allows the input data for the two codes to be easily integrated. (see Appendix A)

The second consideration driving the choice of elements was the goal of the finite element analysis. The output data of interest were nodal translations. The CTRIA3 element proved to have adequate accuracy in this respect, eliminating the need for a more refined element.

The CTRIA3 Element. The CTRIA3 element is formed by combining a constant strain triangle with an isoparametric triangular bending element. (7:5.8-2 - 5.8-16) The resulting element has six degrees of freedom at each node. Defining a local coordinate system such that the local x and y axes lie in the plane of the triangle, one has for each node:

- u and v displacements in the plane of the element
- out of plane displacement w
- θ_x and θ_y rotations about the local x and y axes

The sixth degree of freedom at each node, rotation about the local z axis, is not supported (has zero stiffness) by this element.

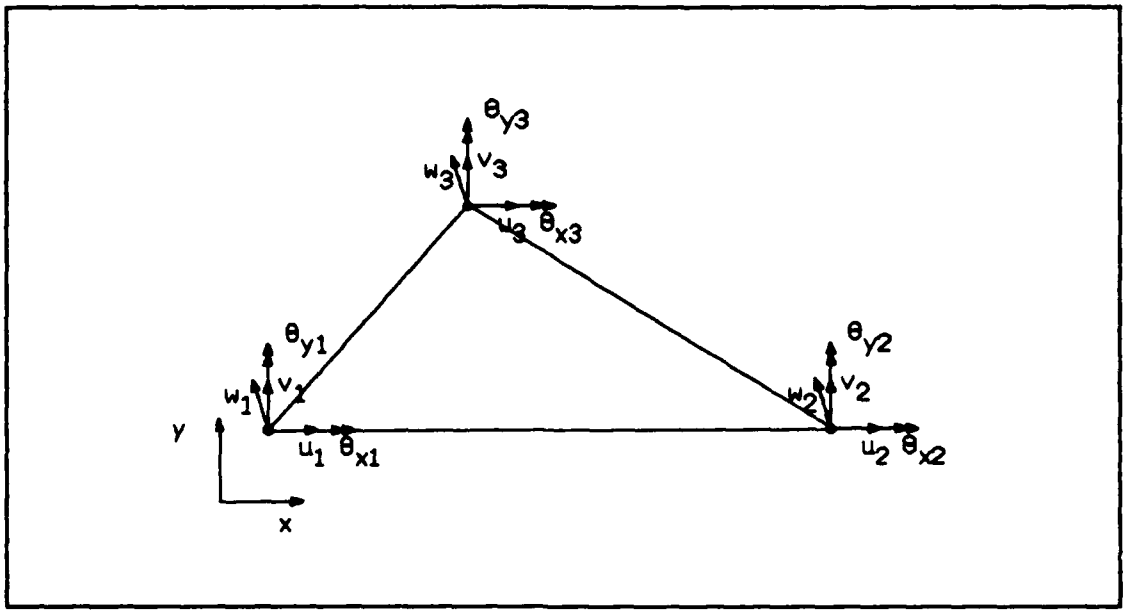

Figure 12. MSC/NASTRAN CTRIA3 Element

When a curved shell structure is being modeled, the process of assembling the stiffness matrices of the individual elements into the global stiffness matrix results in a net stiffness for the (local) θ_z degree of freedom, provided the elements sharing the node do not lie in the same plane.(3:272-274) This occurs because the θ_z degree of freedom for one element at a node has components in the θ_x and θ_y directions when viewed from the reference frame of the other elements at the node.

When a flat plate it is being modeled, transformation from local to global coordinates does not result in any net stiffness in the θ_z degree of freedom. It is therefore necessary to remove this degree of freedom from the model. This is achieved in MSC/NASTRAN by means of the Single Point

Constraint, or SPC card (10:2.4-404), or by means of the PARAM AUTOSPC (10:2.4-286) command.

The flat triangular element does have its limitations and faults. It performs reasonably as a plate element but requires a very fine mesh to obtain good results when used as a shell element. (Reference 2 provides a good example of the successful use of flat triangular element for a spherical shell.) In the next chapter, the models used in this analysis are discussed and the performance of each one is verified.

III. Model Development and Validation

Introduction

In this chapter, the various models used to test the iterative method described in the previous chapter are discussed. Before proceeding, however, it is important to discuss the goals of the analysis and the modeling requirements needed to meet those goals.

The focus of this study was the development of the software necessary to implement the iterative solution to the aeroelastic problem. The analyses performed in support of this work reflect this focus. Testing of the solution technique is given precedence over the actual results. Because of this, the modeling requirements one would normally associate with an analysis of this sort are somewhat relaxed.

Model requirements

The models used to test the iterative method were required to have two characteristics. First, they had to respond to structural loads in a reasonably accurate fashion. The second, perhaps more important requirement, was that they provide accurate answers when placed in the aerodynamic solution.

The second is considered the more important of the two due to the nature of the possible errors involved. In a

finite element analysis of the types of structures studied here, errors are more likely to be quantitative than qualitative. In other words, while the magnitudes of the displacements calculated may be too low or too high, the resulting shape will be more or less correct. When the potential solution is badly modeled, however, the resulting errors completely invalidate the model. An example of this is seen below.

Flat Plate Wing Models

Two models are used to test the solution technique applied to thin lifting surfaces. (Figures 6 and 7) These are flat plate wings, one with unit aspect ratio and one with aspect ratio of 6. The unit aspect ratio wing is used to examine the change in aerodynamic moments and forces associated with static stability derivatives. It is also used to compare iteration convergence rates. The high aspect ratio wing is compared with the one dimensional aeroelastic theory developed in Chapter II.

Each of the wings is modeled as aluminum with Young's Modulus (E) of 10.6E6 psi and Poisson's ratio (ν) of 0.33. Model one is 1/16th of an inch thick and Model two is 1/8th of an inch thick. Model one is four inches square. Model two has a span of 18 inches and a chord of 3 inches.

To determine the theoretical response of the plate to an applied moment, the assumptions made by one-dimensional

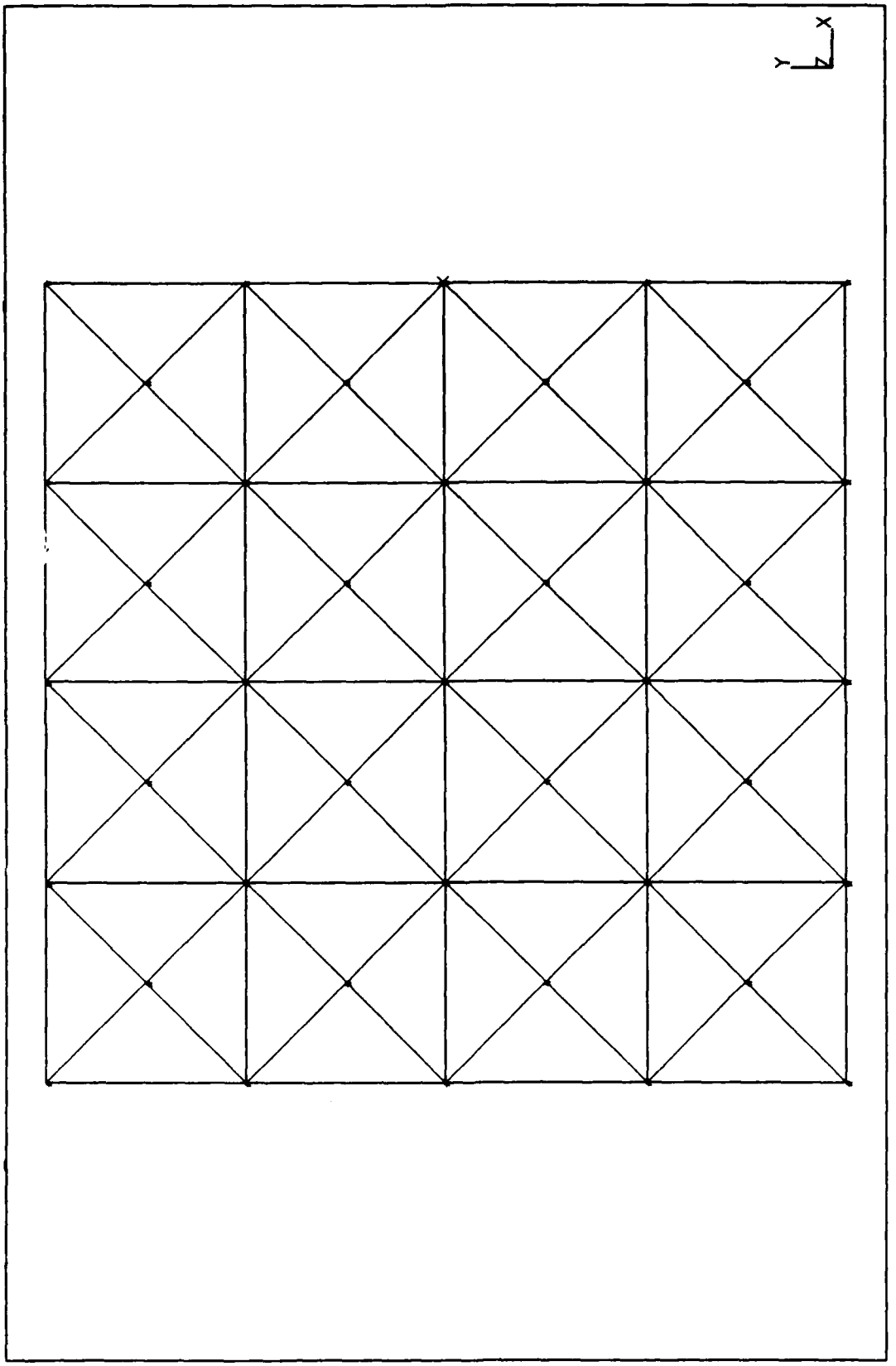

Figure 6. Unit Aspect Ratio Wing (model one)

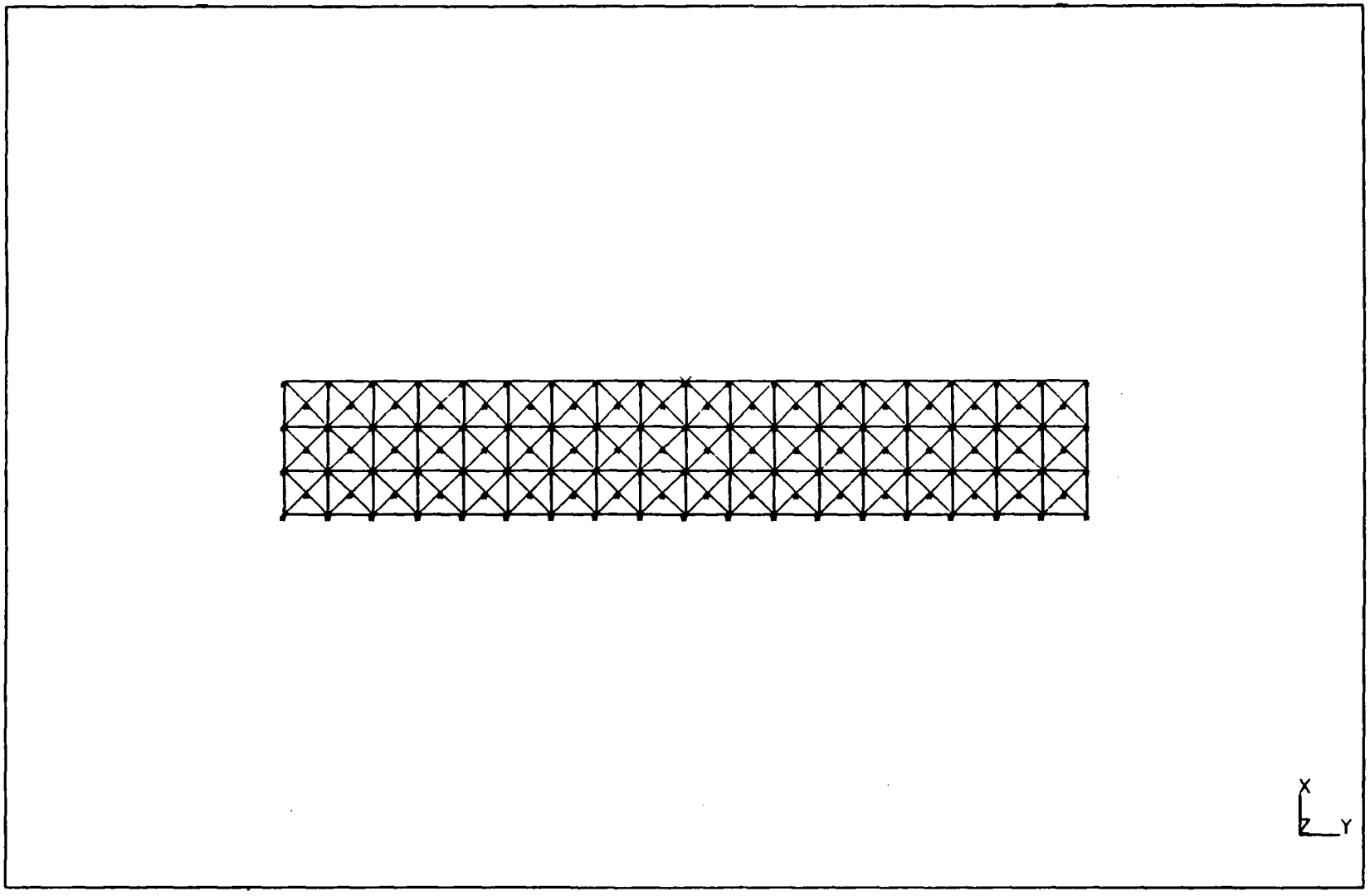

Figure 7. Aspect Ratio Six Wing (model one)

aeroelastic theory are used, i.e., the wing is assumed to behave like a torsion rod and a pure bending beam. The root of each wing is clamped.

For a torsion rod, the rotation about the elastic axis due to a moment applied at an end is

$$\theta_y = \frac{My}{GJ} \tag{3.1}$$

where M is the magnitude of the applied moment, y is the distance along the y axis from the center or root, G is the shear moment, and J is the circular moment about the y axis. Substituting for J as previously defined in Chapter II, the angular deflection at the tip due to an end moment is

$$\theta = \frac{3M\ell}{ch^3G} \tag{3.2}$$

Table I shows the result of applying a 1 foot-pound moment to one end of each of the models. The moment was modeled by applying a linearly varying force to each of the tip nodes in such a manner that a net moment about the centerline of 1 foot-pound resulted. As can be seen, the model adequately models the torsional properties of the plate.

Bending response is tested by applying loads totaling 1 pound to the tip nodes. The resulting displacements are compared to those predicted by beam theory, modified to account for Poisson effects. For a clamped beam with an end load, the tip displacement is (5:92)

Table I. Angular Deflections Due to a 1 Ft Lb End Moment

Model	Rotations (Rad) FEM	Theory	Percent Difference
AR = 1	0.015	0.0185	-19
AR = 6	0.0135	0.0139	-2.8

$$w_{tip} = \frac{4W\ell^3\left(1 - \nu^2\right)}{c\, h^3\, E} \qquad (3.3)$$

where W is the magnitude of the load and ℓ is the semispan of the wing. The results are listed in table II.

Table II. Deflection Due to a 1 Lb end Load

Model	Displacements (in) FEM	Theory	Percent Difference
AR = 1	0.00281	0.00275	+2
AR = 6	0.0452	0.0418	+8

Because the unit aspect ratio model bears little resemblance to a beam, the test results differ from the theoretical values. As this model will be used for qualitative studies, the results are acceptable. The high aspect ratio wing conforms closely to the theoretical values. This model will be used for comparisons to one-dimensional aeroelastic theory.

Spherical Models

The sole purpose of the spherical model is to test the ability of the iterative technique to converge when used for a general shell structure. A moderately fine model is therefore required to sufficiently predict displacements, though not as fine a model as would be required for a complete structural analysis.

Two model configurations were tried. (Figures 8 and 9) At first glance, model one would appear to be preferable to model two. Element size and shape are more consistent and there is a greater degree of symmetry. It turns out, however, that model one could not adequately satisfy the no penetration conditions in the aerodynamic solution. The configuration in model two is used for the following analyses.

Convergence of the Spherical Model. To determine the mesh size required to achieve accurate displacements, a convergence study was conducted. The study was performed by analyzing the deformations of the sphere under a uniform internal pressure for increasingly fine meshes.

The sphere modeled has a radius of 1 meter and a wall thickness of 5 millimeters. The material modeled was an aluminum alloy with Young's modulus (E) of 70.0E+3 MPa, and Poisson's ratio (ν) of 0.33.

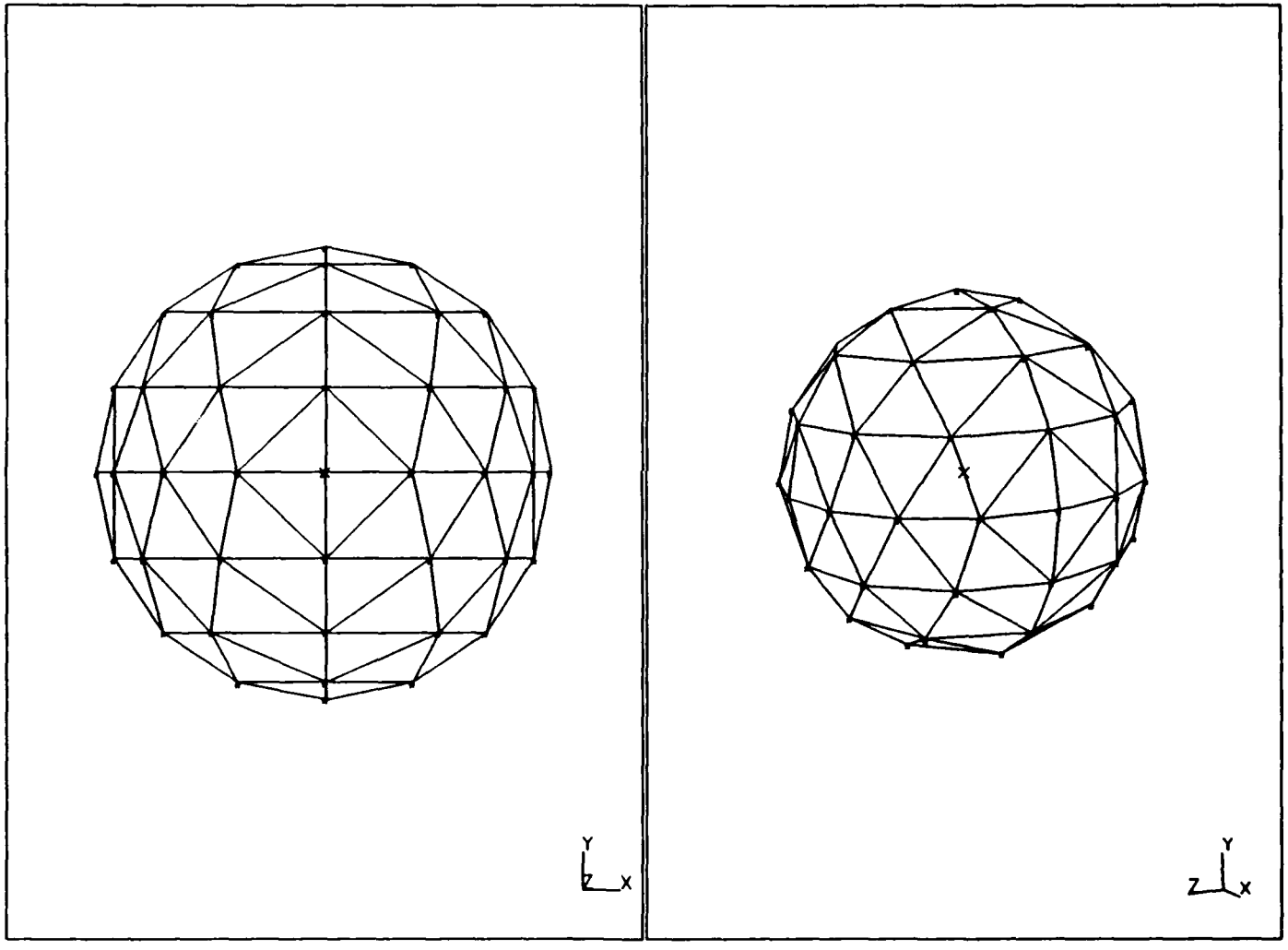

Figure 8. Sphere Model (configuration one)

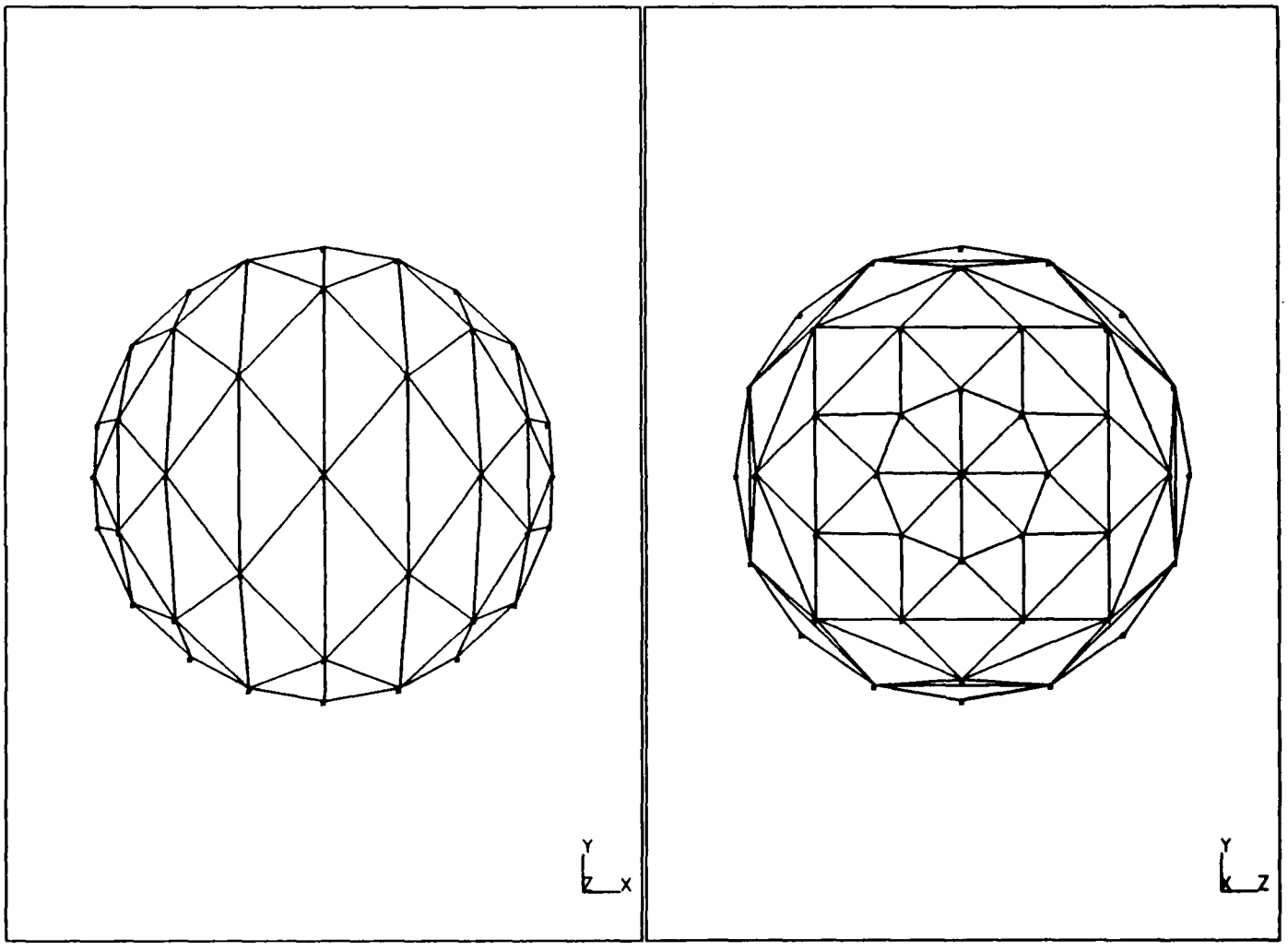

Figure 9. Sphere Model (configuration two)

The theoretical deformation of an isotropic sphere under uniform internal pressure can be obtained from strength of materials arguments as developed in Hearn. (5:202-203) For a sphere deforming due to internal pressure, the change in internal volume equals the original internal volume times the volumetric strain. Assuming that the change in volume is due primarily to the increase in radius of the sphere, the final radius is easily found.

Hoop stress for the sphere is simply

$$\sigma_H = \frac{pd}{4t} \tag{3.4}$$

where p is the internal pressure, d is the diameter of the sphere, and t is the wall thickness. Volumetric strain equals the sum of 3 equal mutually perpendicular strains

$$\varepsilon_v = \frac{3}{E}\left(\sigma_H - \nu\sigma_H \right) \tag{3.5}$$

$$\varepsilon_v = \frac{3pd}{4tE}\left(1 - \nu \right) \tag{3.6}$$

The change in internal volume is then

$$\Delta V = \frac{3pd}{4tE}\left(1 - \nu \right)V_i \tag{3.7}$$

Noting that the final volume is

$$V_f = V_i + \Delta V \tag{3.8}$$

$$V_f = V_i\left[1 + \frac{3pd}{4tE}\left(1 - \nu \right) \right] \tag{3.9}$$

the final radius may be calculated as

$$r_f = \left[r_i^3 \left[1 + \frac{3pd}{4tE}\left(1 - \nu \right) \right] \right]^{\frac{1}{3}} \qquad (3.10)$$

The change in radius Δr is simply $r_f - r_i$. Substituting in the appropriate values one finds the theoretical change in radius is 0.957 E-4 M = .957 mm.

Spherical models were analyzed containing 144, 312, 544, and 840 elements. To simplify evaluation of the results, care was taken to ensure that nodes rested on each of the x, y and z axes. The model was restrained by allowing these nodes to move only along their respective axes. This restraint method ensured that all motion would be fully symmetrical.

Figure 10 shows the results of the convergence test as percent error in displacement magnitude vs latitudinal angle (measured from the x axis). As can be seen, the model is converging to the theoretical solution as it is refined. The 544 element model was chosen for the aeroelastic analysis.

Missing from Figure 10 are the errors at the poles. These points proved to be bad points in the model. Displacements at these points were typically 100 percent higher than theoretical, and worsened as the model was refined. The nodes simply had too many elements (ranging from 8 to 20) attached to be modeled accurately. In

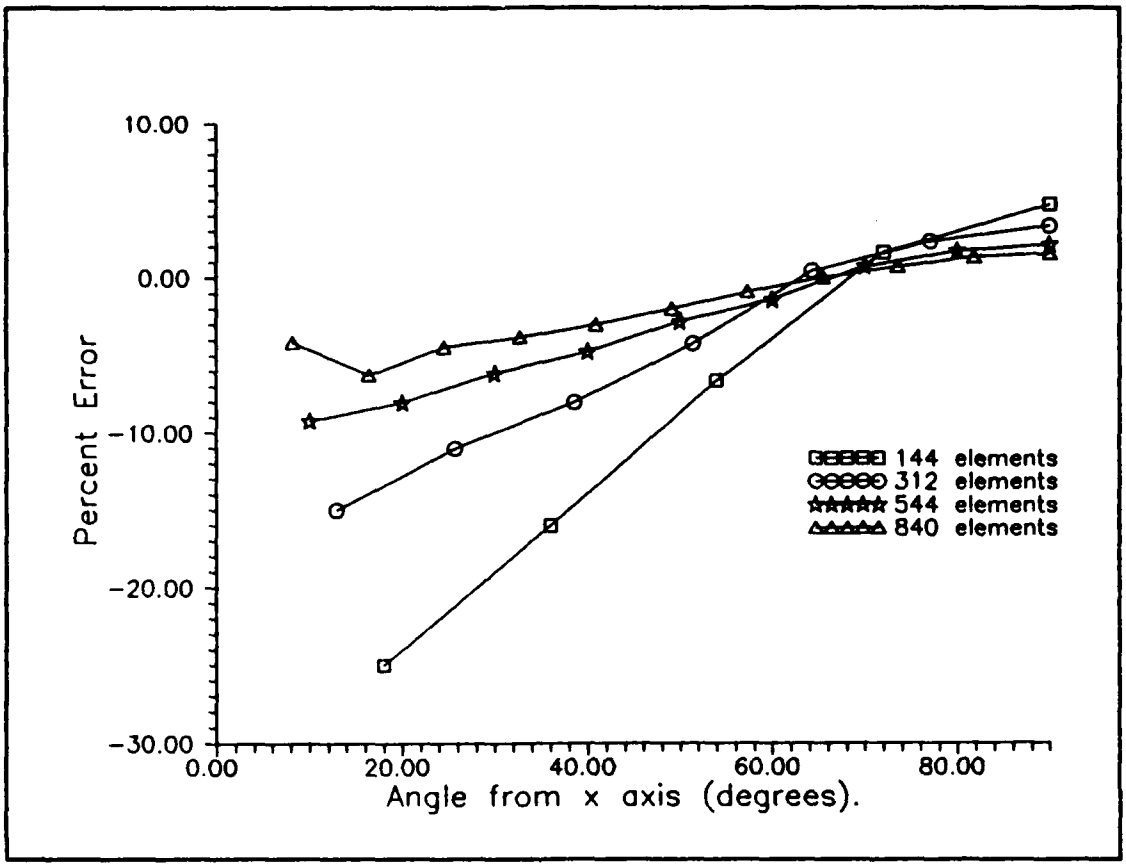

Figure 10. Error in Displacement Magnitude for Varying Mesh Density.

addition, the elements were much smaller and had higher aspect ratios than other elements in the model. This led to a region of the model which was laterally much less rigid than other regions of the sphere, resulting in large deflections.

To estimate the effect of the two bad nodes on the overall behavior of the sphere, the nodes were forced to displace the theoretical amount. Figure 11 shows the results of this test for the 312 element model. It is clear

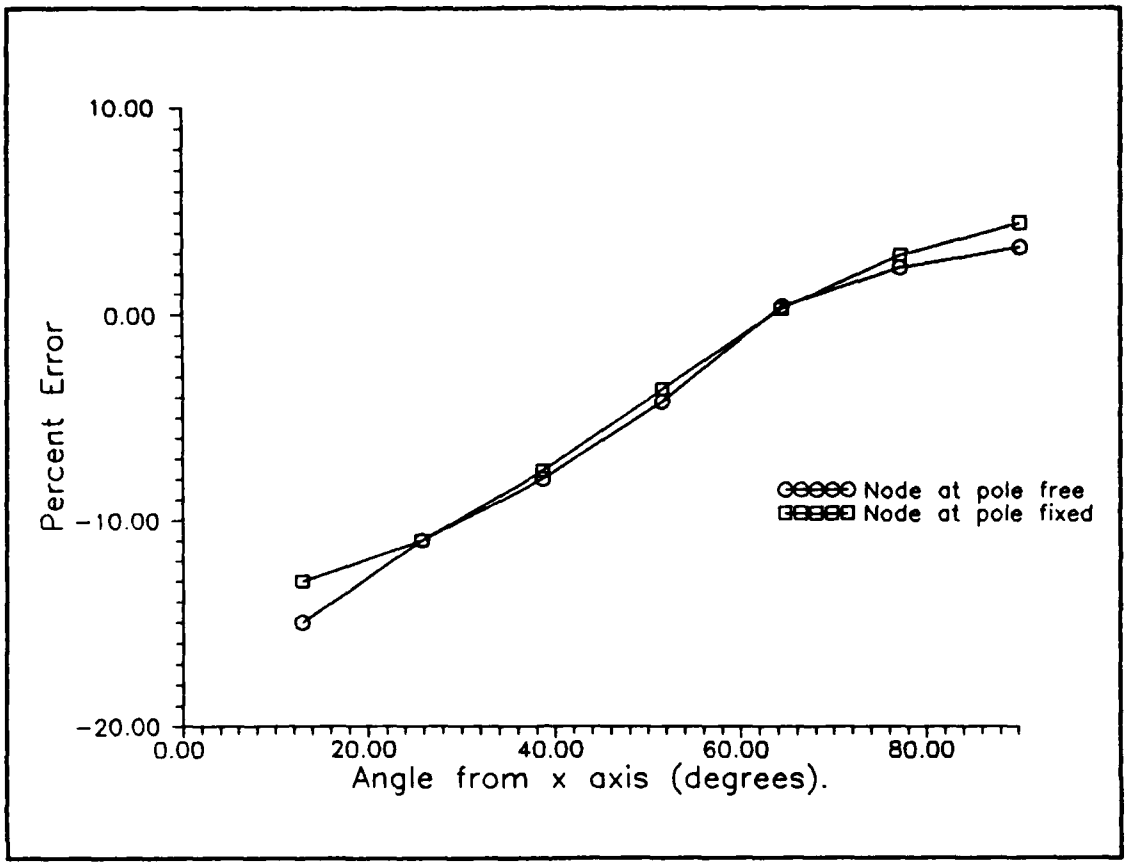

Figure 11. Effect of Error at Poles for 312 Element Sphere

that the nodes have a very small effect on the overall behavior of the model.

The errors experienced at the poles for a uniform pressure loading will have little effect on the aeroelastic analysis because they lie on the stagnation points of the flow. Lateral loads at the points are very small, minimizing the influence of the nodes on the analysis.

IV. Discussion and Results

Introduction

In this chapter, the results of the analyses conducted to test the iterative solution technique are presented and discussed. Before discussing the results, however, the performance of the solution technique itself is examined.

Evaluation of the Iterative Technique

Whenever a technique for solving a problem is developed, there are two evaluations which must be made. One, obviously, is an evaluation of the quality of the results provided by the solution. The second, sometimes overlooked evaluation, is of the solution technique itself. How a solution behaves can be as important as the results it gives.

Speed. The time required to generate results is an important factor when evaluating a means of solving a problem. Much effort was spent in the development of the present method to improve performance in this area.

Because MSC/NASTRAN, a commercial software package, is used for the structural analysis portion of each iteration, attempts to reduce the overall running time of the method were limited to changes in the aerodynamic code. Of the many changes made, the one with the largest impact on

execution time was the row-echelon reduction of the constraint equations discussed in Chapter II.

For moderately large models, the time required to complete an iteration is dominated by the solution of the matrix equations 2.33 and 2.34. For the 216 element wing model, the original method of solution resulted in a linear system of 302 equations which had to be solved each time step. After row-echelon reduction, this system is reduced to just 95 equations. Because the time required to solve N simultaneous equations is proportional to N^3, solution of the reduced set takes approximately 1/30th the time required to solve the original set.

Other, less dramatic, improvements in performance were obtained by modifying several of the key subroutines to make them more efficient. These modifications resulted in 15 to 35 percent reductions in execution time, depending on the size of the model and the number of time steps used.

Despite these improvements, the aerodynamic solution is still very computationally intensive, and requires a very fast computer to implement realistically. The 216 element wing required from three to nine hours per iteration (50 time steps) on an ELXSI 6400 supermini computer.

Convergence Rate. Another factor in the time required to generate results is the rate of convergence. Convergence rate was found to be dependent on the relative magnitude of aeroelastic distortion. As the magnitude of the nodal

displacements increased, so did the number of iterations required to reach equilibrium. Table III lists the number of iterations required for the three test models under varying conditions. The maximum relative displacements are generated by dividing the maximum nodal displacement by the radius (sphere) or the semispan (wings).

Table III. Iteration Convergence Rates for Various Models

Model	Max Rel. Displacment	# Iterations
Sphere	0.0000244	3
Wing AR=1,α=5°	0.00011	4
Wing AR=1,α=20°	0.00079	5
Wing AR=6,α=5°	0.0021	7

Sensitivity to Input. As pointed out in Chapter II and demonstrated in Chapter III, the aerodynamic solution may fail for some model geometries. Another, less serious, problem appears as the nodal positions are perturbed from iteration to iteration. The problem arises due to a numerical ambiguity in the subroutine which performs the row-echelon reduction of the constraint equations.

When the constraint equations for an undeformed model are reduced, some number of unknowns are determined to be dependent on the other unknowns, and are eliminated. Unknowns are eliminated when the corresponding column in the

coefficient matrix, with the exception of the diagonal term, are reduced to near zero values. The zero cutoff constant is specified by the input data. As the body is deformed, the same dependency relationships should be found, but small changes in the nodal positions can push values in the columns which should not be eliminated below the specified cutoff value. This results in an incorrect solution based on false dependencies.

This problem appeared with the high aspect ratio wing and with the sphere model. Both models successfully completed the first iteration, but failed to give proper answers on the second iteration. Increasing the magnitude of the zero cutoff value resolved the problem for both models.

While this problem is solvable, it is troublesome as it makes automation of the iterative process uncertain. It is necessary to check after each of the early iterations to insure that the proper number of equations is being solved. One solution would be to append a data card specifying the number of independent unknowns for the initial iteration to the restart file. Later iterations could then automatically modify the zero cutoff value if an error is detected. Using this technique, it would only be necessary to manually check the results of the first iteration.

Overall, the qualitative performance of the iterative technique is satisfactory. Convergence is achieved in a

small number of iterations, and run times, while not short, are not unreasonably long. Before declaring the solution method a success, however, it is necessary to achieve good results. In the next section, the quantitative performance of the technique is evaluated.

Evaluation of Numerical Results

The solution technique was tested by analyzing several model configurations under different conditions. Each configuration was intended to reveal a different aspect of the aeroelastic solution and its effects on the model. The physical properties of the models are described in Chapter III.

Results for the High Aspect Ratio Flat Plate Wing. The analysis of the high aspect ratio wing was designed to allow comparison with one-dimensional aeroelastic theory. Three runs, at three different velocities, (dynamic pressures) were performed. Wing orientation was fixed at five degrees angle of attack. To ensure that steady state conditions were reached, a minimum of 50 time steps were used in the aerodynamic analysis.

For the first run, $\bar{q}$ corresponds to a low mach number. The second run corresponds to a mach number of .7, the maximum allowed in potential flow theory. A third run was made with the velocity set midway between the first two. An analysis near the divergence dynamic pressure was not

possible for this wing, because divergence occurs at supersonic velocities. A value of 4.2 is used for C_{l_α}. (12:77)

Figure 12 is a displacement contour map for the deformed wing at high mach number. It clearly shows the characteristic deformation of a wing, with the point of maximum deflection at the tips of the leading edges. Figure 13 shows the same wing in a head on view, with displacements magnified to make them visible.

Tables IV and V compare the calculated angular and bending displacements at the wing tips with those predicted by one-dimensional theory for each of the dynamic pressures. The tables indicate a sizable discrepancy between the calculated and theoretical values. These discrepancies are not unexpected.

The one-dimensional equations were developed under the assumption that the lift distribution along the span is constant. This assumption would be correct for an infinite wing, but for a finite wing, tip effects occur. The lift distribution decreases from a maximum at the root to zero at the tips. Figure 14 shows the lift distribution for an elliptical wing. The distribution for a rectangular wing exhibits similar behavior.

Because the lift on a finite wing falls off as the tips are approached, the magnitude of the forces, and thus the

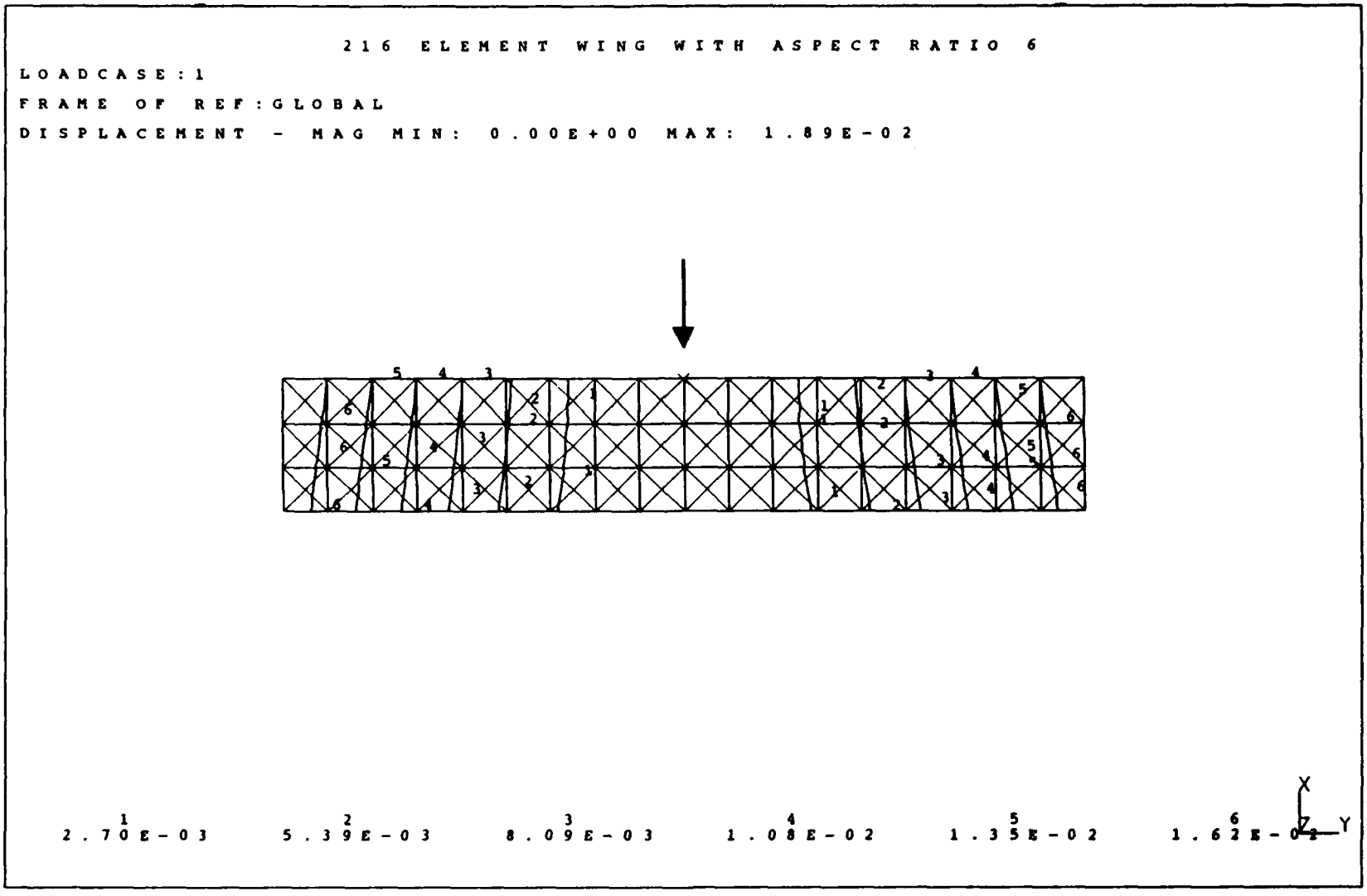

Figure 12. Displacement Contour Map for High Aspect Ratio Wing at Mach Number of 0.7

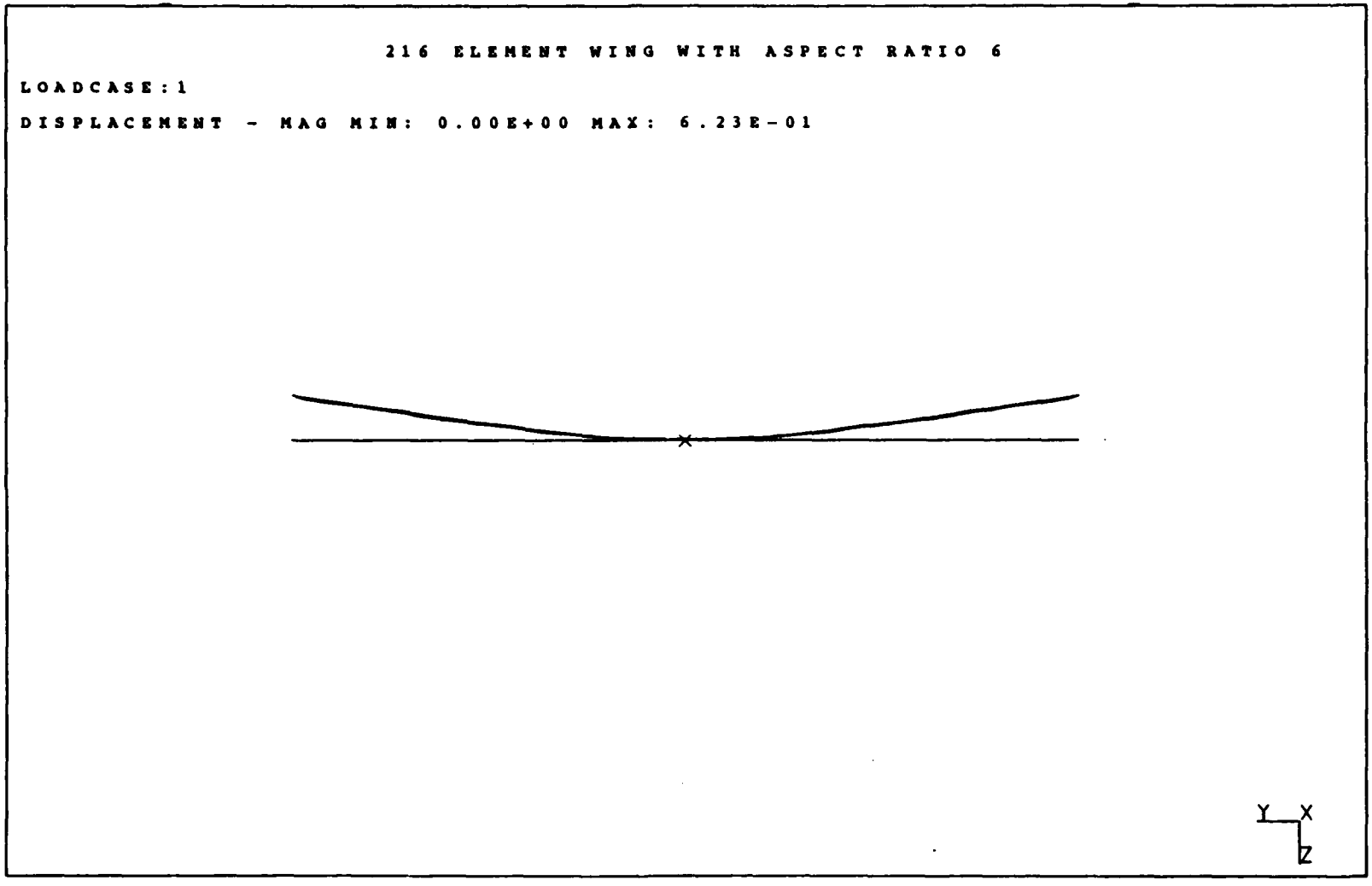

Figure 13. Front View of Deformed High Aspect Ratio Wing for Mach Number of 0.7

Table IV. Angular Displacement at the Wing Tips with Changes In Dynamic Pressure (AR=6)

$\bar{q}$	Rotations (rad) Theory	Calc.	Percent Difference
0.1776	0.0007679	0.0003595	-53
1.8	0.008362	0.003843	-54
5.1	0.02796	0.01164	-58

Table V. Bending Displacement at the Wing Tips with Changes In Dynamic Pressure (AR=6)

$\bar{q}$	Displacements (in) Theory	Calc	Percent Difference
0.1776	-0.2786	-0.1834	-34
1.8	-0.3052	-0.1974	-35
5.1	-1.03	-0.606	-41

moments, acting farthest from the wing root are reduced. The result is smaller angular and bending displacements than would be produced by a constant lift distribution. Also, because there is less twist at the wing tips, the lift near the tips is reduced, which further reduces the actual bending displacement.

The finite wing lift distribution is independent of velocity, so one would expect the discrepancies between one-dimensional aeroelastic theory and the calculated

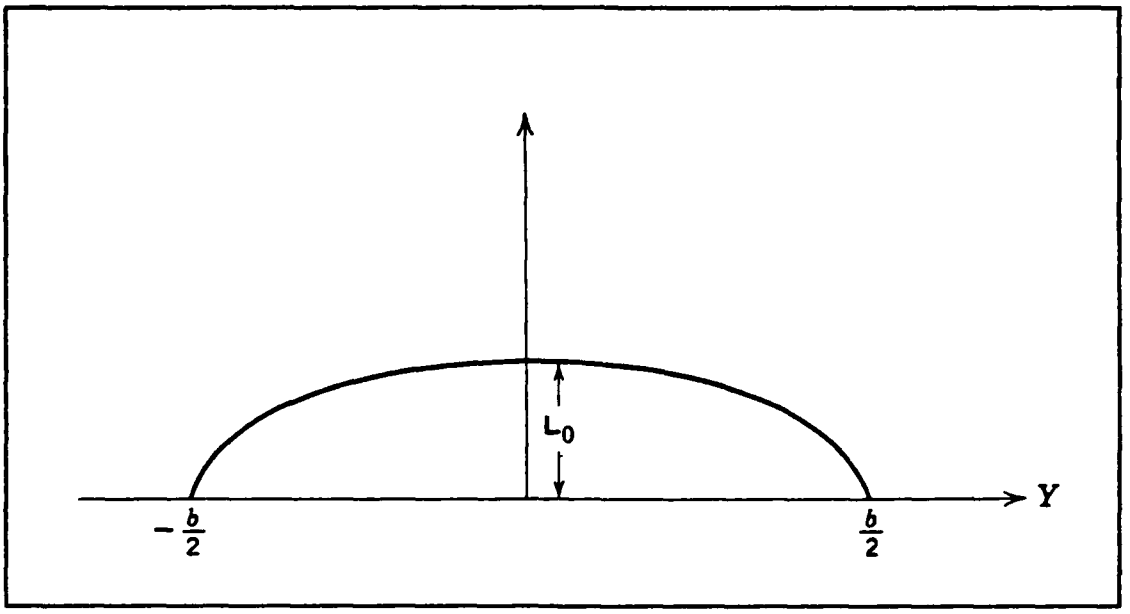

Figure 14. Spanwise Distribution of Lift for An Elliptical Wing

results to be independent of velocity. Tables IV and V support this.

Taking the above considerations into account,the results obtained for the high aspect ratio wing are reasonable. Further validation of the numerical results requires comparison with a more sophisticated aeroelastic theory and is beyond the scope of this work.

Results for the Unit Aspect Ratio Flat Plate Wing. The aerodynamic code used in the iterative solution was originally written for use in an aerodynamic-dynamic simulation of a wing at high angles of attack. (Reference 8) The force and moment coefficients acting on the wing play an important part in such an analysis. To determine, qualitatively, the effect of aeroelasticity on the force and

moment coefficients, a unit aspect ratio wing is analyzed for varying angles of attack. A case with sideslip is also investigated.

Figure 15 shows the deformed wing for α_o= 20. Displacements have been magnified to make them easily visible. Figure 16 is a displacement contour plot of the same wing. These figures illustrate the aeroelastic deformations that affect the wing stability derivatives.

The increased angle of attack at the wing tips will increase both the normal force coefficient and the moment coefficient about the y axis. The change in angle of attack at the wing tip increases with increased initial angle of attack. One therefore expects aeroelastic effects to be more prominent at higher angles of attack. Tables VI and VII illustrate this relationship.

Table VI. Change in the Normal Force Coefficient due to Aeroelastic Effects at Various Angles of Attack

α_o (degrees)	C_{f_z} (undef)	C_{f_z} (def)	% Change
2	-0.045286	-0.045293	0.015
5	-0.13917	-0.13920	0.022
10	-0.33774	-0.33784	0.029
15	-0.57970	-0.57994	0.041
20	-0.86025	-0.86070	0.052

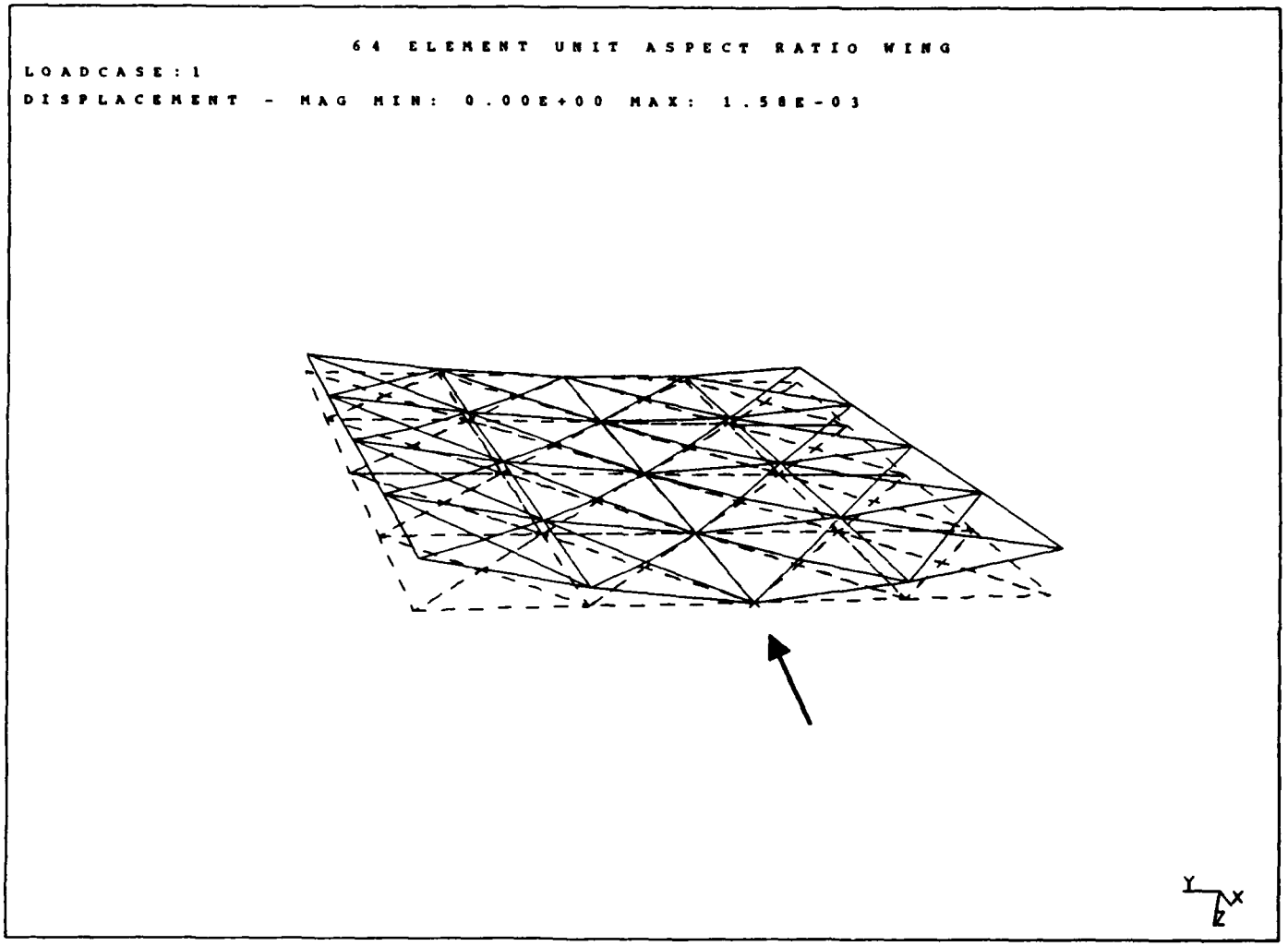

Figure 15. Deformed Unit Aspect Ratio Wing, 20 Degrees Angle of Attack

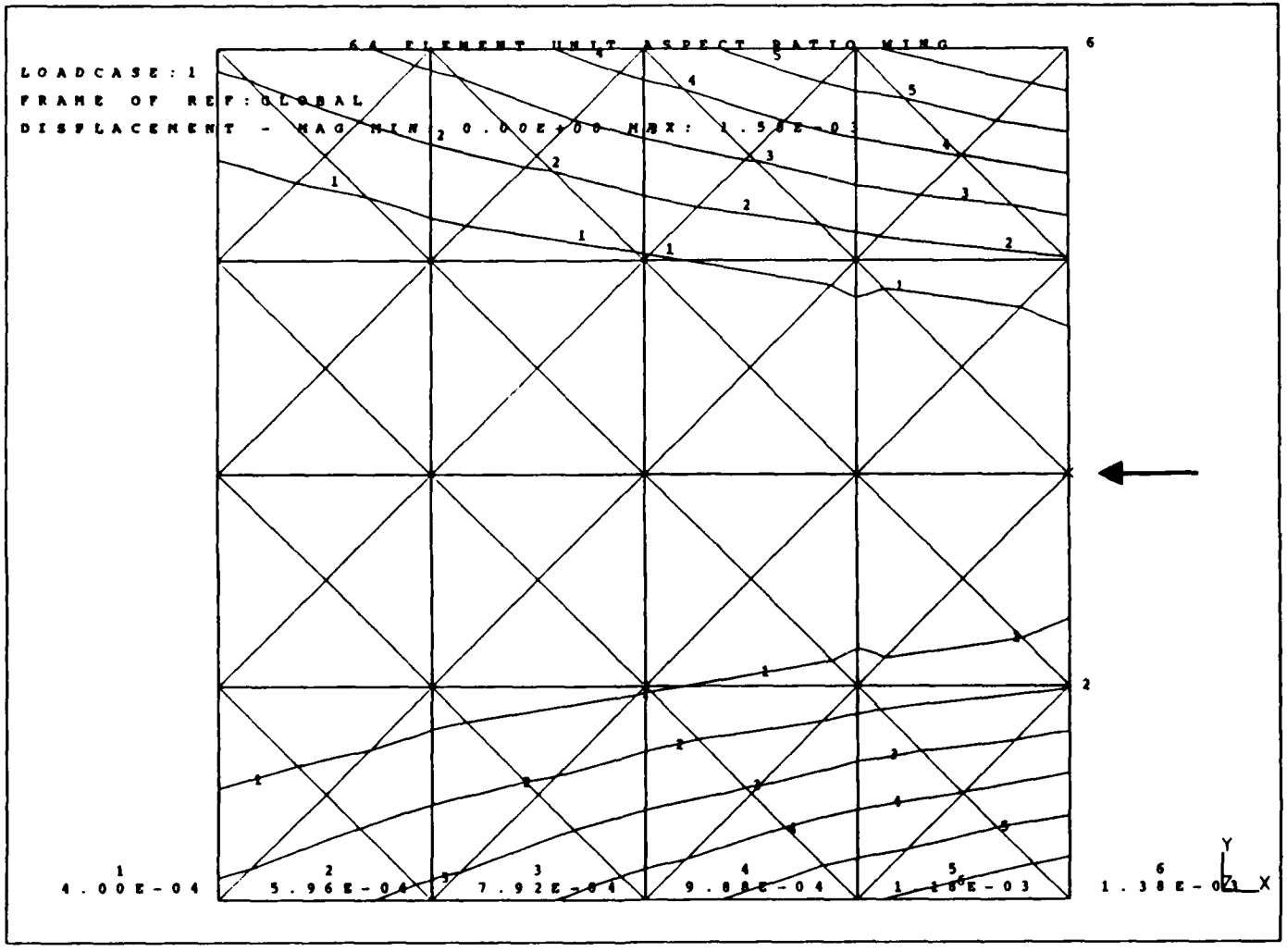

Figure 16. Displacement Contour Plot, Unit Aspect Ratio Wing, 20 Degrees Angle of Attack

Table VII. Change in the Y Moment Coefficient due to Aeroelastic Effects at Various Angles of Attack

α_o (degrees)	C_{m_y} (undef)	C_{m_y} (def)	% Change
2	-0.0081723	-0.0081732	0.011
5	-0.032131	-0.032139	0.025
10	-0.087028	-0.087056	0.032
15	-0.15431	-0.15437	0.039
20	-0.23004	-0.23015	0.048

It is clear from these results that the current method is capable of estimating the effects of aeroelasticity on the factors affecting aircraft stability and control. In its current state, the iterative technique could be used to perform a quasi-static (no inertia effects) analysis of a structure in various flight conditions. Indicated corrections could then be applied to the rigid body stability and control derivatives.

Results for a Sphere. To test the iterative technique on a non-lifting, closed shell structure, a sphere was modeled and analyzed. Figure 17 shows the model before and after deformation.

The pressure distribution over a sphere in potential flow is given by $1 - 9/4\sin^2(\theta)$ (6:349), where θ is the angle from a point on the sphere to the stagnation point. The air inside the sphere is stationary, and thus is

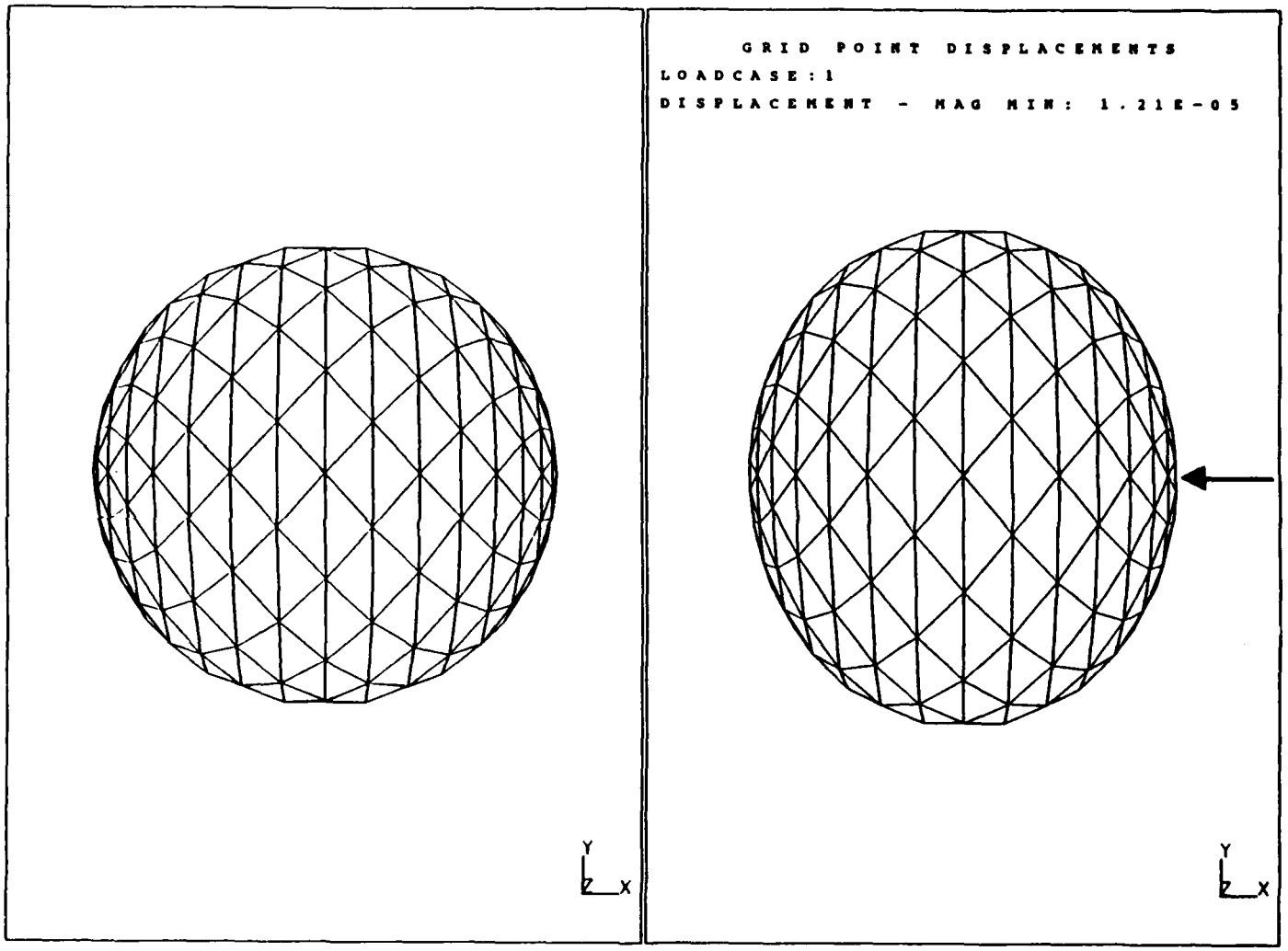

Figure 17. Sphere Model Before and After Aeroelastic Deformation

assumed to have the same pressure as the stagnation points. The difference between the internal and external pressures at all other points (net outward) is the source of the loads which deform the sphere.

The load distribution is proportional to $\sin^2(\theta)$, and thus goes from zero at the stagnation points to a maximum 90 degrees from the stagnation point. This load distribution causes the sphere to flatten out as shown in Figure 17. As the sphere flattens the pressure near the stagnation points increases, and the pressure near the 90 degree mark decreases. These changes were calculated and are presented in Table VIII and plotted in Figure 18.

Quantitative evaluation of the results for the analysis of the sphere is difficult. For a general shell structure it may be impossible. Because of the nature if the iterative solution, however, the results of such an analysis should be capable of achieving a high degree of accuracy. The limiting factor will be the structural model itself.

Conclusions

The analyses discussed above were not intended to be studies in and of themselves, but were intended to test iterative solution technique and explore its capabilities. The results indicate that the technique is capable of solving a wide range of problems in several disciplines, including structural design and stability and control. Further study is necessary to fully establish the

Table VIII. Changes in C_p on a Sphere due to Aeroelastic Deformation

Position (degrees)	Cp (undeformed)	Cp (deformed)	∇ Cp
0	1.000000	1.000000	0.000000
10	0.928974	0.928982	0.000008
20	0.728588	0.728613	0.000025
30	0.421849	0.421890	0.000041
40	0.005132	0.005136	0.000040
50	-0.334272	-0.334250	0.000022
60	-0.686415	-0.686425	-0.000010
70	-0.965099	-0.965143	-0.000044
80	-1.142572	-1.142640	-0.000068
90	-1.203352	-1.203429	-0.000077

capabilities and limits of the method. The next chapter provides suggestions for future study and development of the technique.

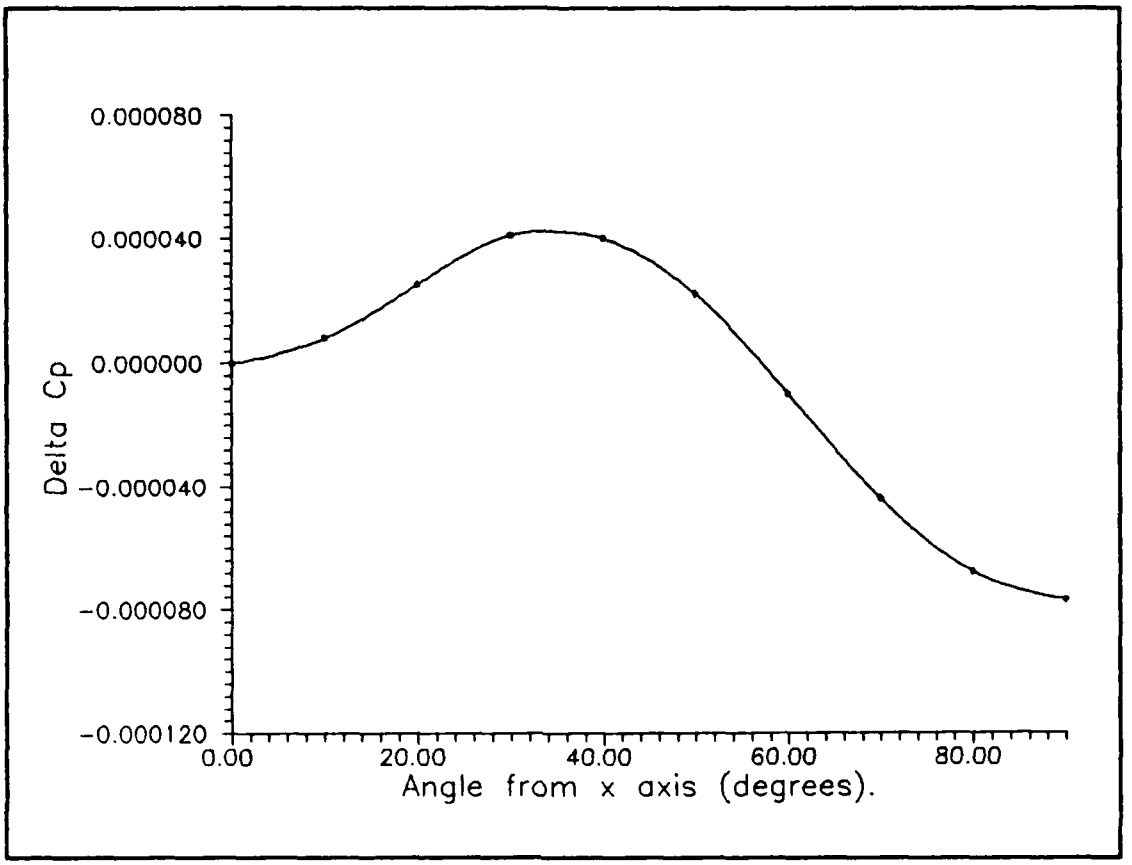

Figure 18. Changes in C_p On a Sphere due to Aeroelastic Deformation

V. Recommendations

Much of this investigation was performed with the intent that this work would serve as the foundation upon which future studies would be built. Many areas exist which would benefit from further study. A few of these are discussed below.

This investigation is limited to static aeroelasticity. The extension of this work to unsteady phenomena would greatly enhance its utility in the field of aircraft stability and control. One possible application is the incorporation of unsteady aeroelastic effects in an aerodynamic-dynamic simulation.

Structural modeling in the current method is limited to a single, relatively primitive finite element. The incorporation of higher degree of freedom elements is necessary before the technique can be used for serious structural analysis. This extension would involve the development of a means of selectively breaking those elements down into the basic triangle required by the aerodynamic code, or in the case of internal elements, hiding them from the aerodynamic solution. The incorporation of non-linear elements would further enhance the method.

Appendix A: Interface Between MSC/NASTRAN and the Potential Flow Code

This appendix describes the development and use of the interface between MSC/NASTRAN and the aerodynamic code.

Due to the iterative nature of the aeroelastic solution, it is desirable to have a single model for both the aerodynamic and the finite element analysis. Because the two programs share many data requirements, this is fairly easy to implement.

Common between the two programs is the content of geometric data. Both programs use a three noded triangular element which requires nodal positions (x,y,z coordinates) and element connectivity information. The data input routines for the aerodynamic code were rewritten to accept this information in the form of MSC/NASTRAN GRID and CTRIA3 cards. In addition to the obvious advantage of having a single data format, this change is useful in other ways. There exist many preprocessors which can produce Nastran data files. These programs may now be used to generate model geometry, whether or not an elastic analysis is being done. Post processing for this thesis was performed using SDRC-IDEAS by the Structural Dynamics Research Coproration, Milford OH.

Both MSC/NASTRAN and the aerodynamic code require information not used by both programs. To allow a single input data file for both programs, the MSC/NASTRAN comment card is utilized. All information required by the aerodynamic code, other than nodal and element information, is input on MSC/NASTRAN style cards, with the name of the card beginning with a dollar sign. This format forces MSC/NASTRAN to read all aerodynamic specific data as comment cards. In like manner, the aerodynamic input routines ignore MSC/NASTRAN specific data. Thus the goal of a single data file for both programs is achieved.

Load information is calculated by the aerodynamic code, and therefore cannot be included in the initial data file. A routine was written and included in the aerodynamic solution which outputs nodal pressures in the form of MSC/NASTRAN PLOAD4 cards. See Reference (10:2.4-325) for more information on this card.

During the iteration process, the interface between MSC/NASTRAN and the aerodynamic codes works as follows:

1. A single file containing all data necessary for both programs is created.

2. The input file is read into the aerodynamic code. Two copies of the input file are created as it is read. The first is a restart file that will be used to start the next iteration. The default name of this file is

<filename>.r##, where <filename> is the root name of the input data file, and ## indicates the iteration number. The second file created is the MSC/NASTRAN data file which includes the generated PLOAD cards. The default name for this file is <filename>.n##.

3. MSC/NASTRAN is used to generate a nodal displacement file using the previously generated .n## file. The original data file should have the statement

DISPLACEMENT(PUNCH)=ALL

in the MSC/NASTRAN case control deck.(10:2.3-20). Nodal displacements are written to a file named <filename>.PCH, which should be renamed to have a .d## extension.

4. The aerodynamic code is run using the .r## file generated in the previous iteration. The .d## file is automatically read and nodal positions adjusted.

5. Steps 3 and 4 are repeated until no change occurs in the .d## and .n## files from one iteration to the next. Figure 19 contains a flow chart of this process.

Appendix B describes each of the aerodynamic specific data cards, as well as those MSC/NASTRAN Cards required for an aerodynamic only analysis. Appendix C consists of the input data file for a 64 element, unit aspect ratio, flat plate wing. For more information on MSC/NASTRAN Specific input data, see Reference (14) or the MSC/NASTRAN Users Guide (Reference 10).

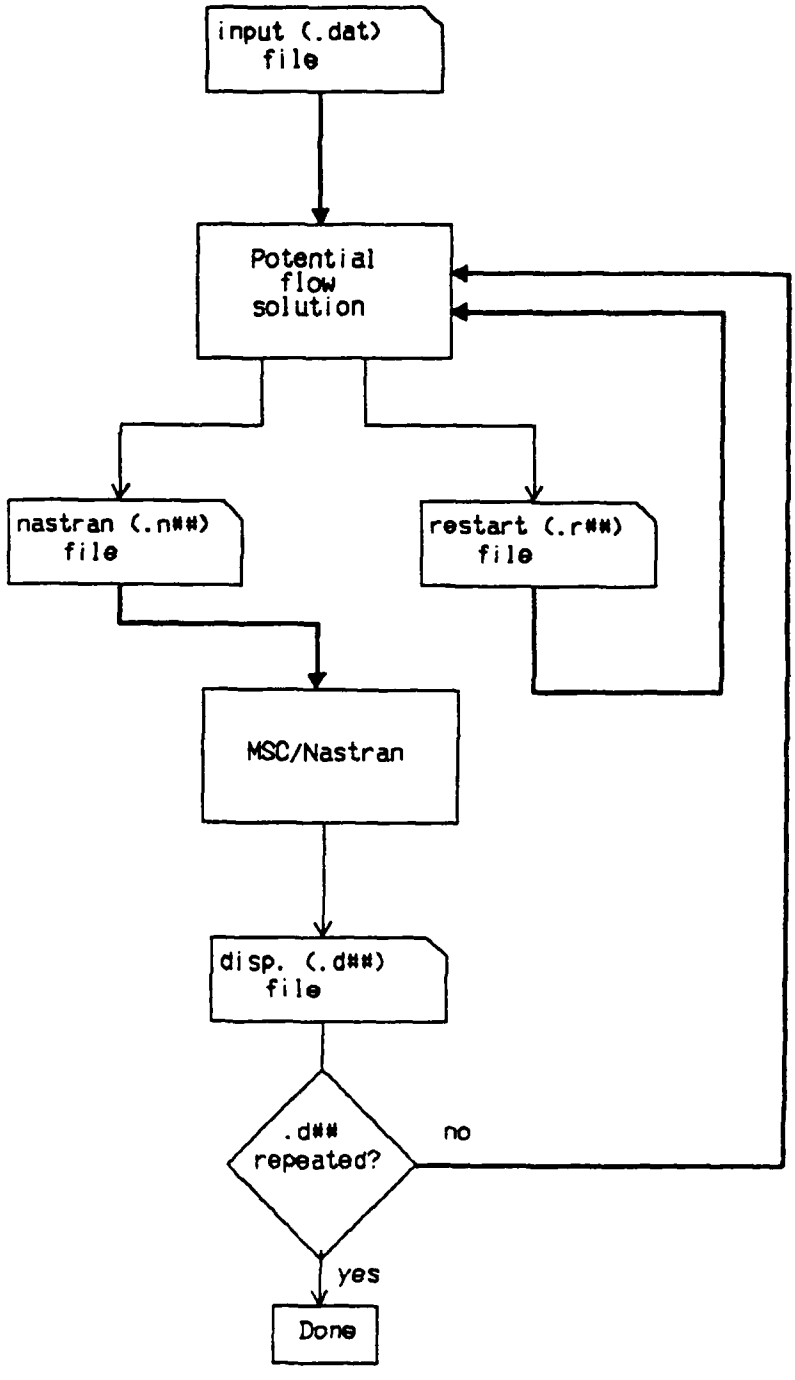

Figure 19. Flow Chart of the Iterative Process

APPENDIX B: Input Data Card Formats

This appendix lists the format for data cards in the model input file. All cards with the exception of GRID, CTRIA3, and ENDDATA are not part of MSC/Nastran and are prefaced with a "$" (dollar sign). Thus they are treated as comments by MSC/NASTRAN. The cards are described in the following format.

CARD NAME: The name of the card.

PURPOSE: A brief description of the purpose of the card.

DESCRIPTION: A field by field description of the card. All descriptions begin with field 2. Field 1, the first 8 characters of the card, always contains the name of the card in capital letters, left justified. Fields may be either long (16 characters) or short (8 characters) and floating point or integer. Type is indicated by the codes f or i. One other field type, file, is found on some cards. Along with the type, the starting and ending columns of each card are given.

REMARKS: Information concerning multiple entries, default values, etc. is listed.

It should be noted that unless otherwise stated, cards may appear in the model file in any order. Cards with multiple entry capability need not have multiple entries. When a default value is indicated for any field, that field may be left blank.

CARD NAME: $AIRPROP

PURPOSE: Input flow constants.

$AIRPROP	2	3	4	5	

DESCRIPITON:

field 2:f(9-24) reference pressure (absolute).

field 3:f(25-40) free stream velocity.

field 4:f(41-56) free stream pressure (absolute).

field 5:f(57-72) density of fluid.

REMARKS: A value of -2.0 for the reference pressure indicates that a thin lifting surface is being analyzed. For values greater than -2.0 the pressure is used as the interior pressure for a closed body. The default reference pressure is -1.0, which is a special value indicating that the flow stagnation pressure should be used.

The default value for the free stream velocity is 100 M/s

The default value for the free stream pressure is 101330 MPa

The default value for the fluid density is 1.225 Kg/M^3

CARD NAME: $CONVEDG

PURPOSE: Specify the convecting edge elements.

$CONVEDG	2	3	4	...					

DESCRIPTION:

field 2:i(9-16) node 1 of convecting edge 1 on card.

field 3:i(17-24) node 2 of convecting edge 1 on card.

field 4:i(25-32) edge circuit identifier.

...

REMARKS: Up to 3 convecting edges may be entered on each card. Node numbers must correspond to nodes defined using GRID cards. The edge circuit identifier refers to a convecting body. (if only one body, then must be 1)

CARD NAME: $CORNER

PURPOSE: Identify the corners on the body.

$CORNER	2	...							

DESCRIPITON:

field 2:i(9-16) corner node.

REMARKS: Up to 8 corner nodes may be defined on each card. Node numbers must correspond to nodes defined using GRID cards.

CARD NAME: CTRIA3

PURPOSE: Define an element (triangle).

CTRIA3	2	-	4	5	6				

DESCRIPITON:

field 2:i(9-16) element (triangle) number.

field 3:i(17-24) (MSC/NASTRAN specific)

field 4:i(25-32) node number of first vertex

field 5:i(33-40) node number of second vertex

field 6:i(41-48) node number of third vertex

REMARKS: This card is an MSC/NASTRAN bulk data card. The element number is a unique number between 1 and the total number of elements. Elements may be entered in any order, but no number should be skipped. Node numbers must be valid nodes entered with a GRID card. The long form (16 character fields) of this card is supported (see the GRID card). For more information, see the MSC/NASTRAN users manual (10:2.4-118).

CARD NAME: $CUTOFF

PURPOSE: Define values to be considered zero

$CUTOFF	2	3	4						

DESCRIPITON:

field 2:f(9-16) effective zero for triangles

field 3:f(17-24) effective zero for wake

field 4:f(25-32) effective zero for row echelon calculations

REMARKS: Effective zero values for triangles and the wake are used to determine proximity to singular values during internal calculations. Default for each is 1.0 x 10-6. The effective zero for row-echelon calculations is used when determining redundant equations. Default is 1.0x10-5. IMPORTANT: If an analysis results in loss of symmetry and poorly satisfied no penetration conditions, it is likely that this value is too high or too low. The reduced number of equations is printed in the .log file, and should remain constant from one iteration to the next.

CARD NAME: $EDGECOR

PURPOSE: Input the starting and ending nodes for the edge vortex cores.

$EDGECOR	2	3	...						

DESCRIPTION:

field 2:i(9-16) node 1 of core 1 on card.

field 3:i(17-24) node 2 of core 1 on card.

...

REMARKS: Up to 4 cores may be entered on each card. Node numbers must correspond to nodes defined using GRID cards.

CARD NAME: $ELASTIC

PURPOSE: Identify the run as an aeroelastic iteration.

$ELASTIC	2	3	4				

DESCRIPITON:

field 2:file(9-24) name of MSC/NASTRAN data file to be written.

field 3:file(25-40) name of displacement file to be read.

field 4:i(41-48) iteration number.

REMARKS: If a filename is supplied for field 2 (3), that file will be created (read). If left blank, the root name of the input data file will be used with the file extension ".n#" or (".d#") where # refers to the iteration number. Field 4 should be blank in the initial data file. It is automatically incremented in the restart file for each iteration.

CARD NAME: $ERRCHK

PURPOSE: Turn on printing of the no penetration error.

$ERRCHK	

DESCRIPITON:

No additional fields

REMARKS: This card is included to aid in evaluating a new model. If the card is included in the input data file, a file named "noPen.err" will be created. This file has the format

"Element: # Error: #.#,"

with one line for each element. The error is calculated by subtracting the calculated velocities normal to the element surface from the actual (inertial) velocity normal to the surface.

CARD NAME: GRID

PURPOSE: Define a node.

Grid	2	-	4	5	6				
GRID*	2		-		4		5		
*	6								

DESCRIPITON:

field 2:i(9-16) node number.

field 3:i(17-24) (MSC/NASTRAN specific)

field 4:f(25-32) x position of node

field 5:f(33-40) y position of node

field 6:f(41-48) z position of node

REMARKS: This card is an MSC/NASTRAN bulk data card. The node number is a unique number between 1 and the total number of nodes. Nodes may be entered in any order, but no number should be skipped. The long form (16 character fields with a continuation line) of this card is supported. It is used by appending an asterisk (*) to the name GRID. Fields 2 through 5 are on the first line. Field 6 is on a continuation line. A continuation line is indicated by an asterisk in column 1 of field 1. For more information, see the MSC/NASTRAN users manual (10:2.4-224).

CARD NAME: $ITERATE

PURPOSE: Flag the body as non planar.

$ITERATE	2								

DESCRIPITON:

field 2:(si) maximum number of iterations.

REMARKS: For models that are non planar or will be deformed, the potential flow solution requires internal iteration. Field 2 contains the maximum number of iterations which may be attempted. The default value is 10.

CARD NAME: $KUTTA

PURPOSE: Identify the nodes where the Kutta condition is to be imposed.

$KUTTA	2	3	...			

DESCRIPITON:

field 2:i(9-16) node.

field 3:f(17-32) Kutta equation weighting factor.

REMARKS: Up to three nodes may be specified on each card. The weighting factor determines the degree to which the Kutta conditions are favored over the no-penetration conditions. A value of 50.0 is typical.

CARD NAME: $ORIENTA

PURPOSE: Input the starting orientation of the body.

$ORIENTA	2	3	4	

DESCRIPITON:

field 2:f(9-16) starting roll angle in degrees

field 3:f(17-24) starting pitch angle

filed 4:f(25-32) starting yaw angle

REMARKS: Default value for each is 0.0 degrees. Card may be omitted if there is no initial angular displacement.

CARD NAME: $POTPATH

PURPOSE: Identify the paths for calculating the potential.

$POTPATH	2	3	4	...					

DESCRIPITON:

field 2:i(9-16) node 1

field 3:i(17-24) node 2

field 4:i(25:32) element used to calculate the potential.

REMARKS: Up to 3 paths may be entered on each card. For a non-convecting body, this card may be omitted.

CARD NAME: $POTSTRT

PURPOSE: Identify starting nodes for the potential paths.

$POTSTRT	2	...							

DESCRIPITON:

field 2:i(9-16) potential starting node.

REMARKS: Up to 8 starting nodes may be defined on each card. Node numbers must correspond to nodes defined using GRID cards. For a non-convecting body, this card may be omitted.

CARD NAME: $TIME

PURPOSE: Input time parameters for the run.

$TIME	2	3	4					

DESCRIPITON:

field 2:i(9-16) number of time steps to run

field 3:i(17-24) number of wake steps to keep

field 4 f(25-40) magnitude of time step

REMARKS: Defaults are 1 time step, 1 wake step, time step = 1.0. For a non-convecting body, this card may be omitted.

CARD NAME: $WAKSTRT

PURPOSE: Input the starting nodes for the convecting wake.

$WAKSTRT	2	...							

DESCRIPTION:

field 2:(si) wake starting node.

...

REMARKS: Up to 8 starting nodes may be defined on each card. Node numbers must correspond to nodes defined using GRID cards. Wake starting positions are taken to be the node positions as defined by the grid cards.

CARD NAME: $WING

PURPOSE: Input the wing constants.

$WING	2	3	4	

DESCRIPITON:

field 2:f(9-24) wing chord

field 3:f(25-40) wing span

field 4:f(41-56) mean aerodynamic chord

REMARKS: For a closed body, this card may be omitted.

Default values are all 1.0.

C. Sample Input Data File

The following input data file defines a flat plate unit aspect ratio wing, four inches square. Flight velocity is set to 1760 inches per second. The angle of attack is 10 degrees. The analysis will run for 60 time steps, keeping 20 wake rows. A Nastran input file with the defualt filename will be produced.

```
$ This a 64 element wing with unit aspect ratio.
$
$ Establish wing and run properties.
$
$WING              4.0            4.0            4.0
$TIME        60     20            1.0
$ORIENTA    0.0   10.0     0.0
$AIRPROP           -2.0         1760.0                        1.145E-7
$
$ Define the edge cores.
$
$EDGECOR      1      2      2      3      3      4      4      5
$EDGECOR      5     14      1     10     14     23     10     19
$EDGECOR     23     32     19     28     32     41     28     37
$EDGECOR     37     38     38     39     39     40     40     41
$
$ Define the convecting edges. (wake shedding edges)
$
$CONVEDG      5     14      1      1     10      1
$CONVEDG     14     23      1     10     19      1
$CONVEDG     23     32      1     19     28      1
$CONVEDG     32     41      1     28     37      1
$CONVEDG     37     38      1     38     39      1
$CONVEDG     39     40      1     40     41      1
$
$ Identify the nodes for wake starting positions.
$
$WAKSTRT      1      5     10     14     19     23     28
$WAKSTRT     32     37     38     39     40     41
$
$ Identify the nodes where the Kutta condition is enforced.
$
$KUTTA       37       50.00000      38       50.00000
$KUTTA       39       50.00000      40       50.00000
$KUTTA       41       50.00000
$
$ Identify the corners of the wing.
$
$CORNER       1      5     37     41
$
$ Identify the starting point and paths for the potential.
$
$POTSTRT      3
$POTPATH      3      2      5      3      4      9
$POTPATH      4      5     13      2      1      1
$POTPATH      1      6      1      2      7      5
$POTPATH      3      8      9      4      9     13
$POTPATH      1     10      4      2     11      2
$POTPATH      3     12      6      4     13     10
$POTPATH      5     14     14     10     15     17
$POTPATH     11     16     21     12     17     25
$POTPATH     13     18     29     10     19     20
```

```
$POTPATH      11      20      18      12      21      22
$POTPATH      13      22      26      14      23      30
$POTPATH      19      24      33      20      25      37
$POTPATH      21      26      41      22      27      45
$POTPATH      19      28      36      20      29      34
$POTPATH      21      30      38      22      31      42
$POTPATH      23      32      46      28      33      49
$POTPATH      29      34      53      30      35      57
$POTPATH      31      36      61      28      37      52
$POTPATH      29      38      50      30      39      54
$POTPATH      31      40      58      32      41      62
$
$ Turn on internal iteration and produce a nastran data deck
$ with default name.
$
$ITERATE
$ELASTIC
$
$  Nastran executive control deck
$
ASSIGN OUTPUT2=wing64.op2,STATUS=NEW,UNIT=12
TIME 10
DIAG 64
SOL 101 $STATIC ANALYSIS
COMPILE SUPER3, SOUIN=MSCSOU
CEND
$
$  Nastran case control deck
$
TITLE = 64 element unit aspect ratio wing
DISPLACEMENT(punch) = ALL
OLOAD = ALL
     SPC =          1
LOAD=1
SUBCASE          1
$
BEGIN BULK
CTRIA3         1       1       1       2       6
CTRIA3         2       1       2      11       6
CTRIA3         3       1      11      10       6
CTRIA3         4       1      10       1       6
CTRIA3         5       1       2       3       7
CTRIA3         6       1       3      12       7
CTRIA3         7       1      12      11       7
CTRIA3         8       1      11       2       7
CTRIA3         9       1       3       4       8
CTRIA3        10       1       4      13       8
CTRIA3        11       1      13      12       8
CTRIA3        12       1      12       3       8
CTRIA3        13       1       4       5       9
CTRIA3        14       1       5      14       9
CTRIA3        15       1      14      13       9
```

```
CTRIA3      16      1      13       4       9
CTRIA3      17      1      10      11      15
CTRIA3      18      1      11      20      15
CTRIA3      19      1      20      19      15
CTRIA3      20      1      19      10      15
CTRIA3      21      1      11      12      16
CTRIA3      22      1      12      21      16
CTRIA3      23      1      21      20      16
CTRIA3      24      1      20      11      16
CTRIA3      25      1      12      13      17
CTRIA3      26      1      13      22      17
CTRIA3      27      1      22      21      17
CTRIA3      28      1      21      12      17
CTRIA3      29      1      13      14      18
CTRIA3      30      1      14      23      18
CTRIA3      31      1      23      22      18
CTRIA3      32      1      22      13      18
CTRIA3      33      1      19      20      24
CTRIA3      34      1      20      29      24
CTRIA3      35      1      29      28      24
CTRIA3      36      1      28      19      24
CTRIA3      37      1      20      21      25
CTRIA3      38      1      21      30      25
CTRIA3      39      1      30      29      25
CTRIA3      40      1      29      20      25
CTRIA3      41      1      21      22      26
CTRIA3      42      1      22      31      26
CTRIA3      43      1      31      30      26
CTRIA3      44      1      30      21      26
CTRIA3      45      1      22      23      27
CTRIA3      46      1      23      32      27
CTRIA3      47      1      32      31      27
CTRIA3      48      1      31      22      27
CTRIA3      49      1      28      29      33
CTRIA3      50      1      29      38      33
CTRIA3      51      1      38      37      33
CTRIA3      52      1      37      28      33
CTRIA3      53      1      29      30      34
CTRIA3      54      1      30      39      34
CTRIA3      55      1      39      38      34
CTRIA3      56      1      38      29      34
CTRIA3      57      1      30      31      35
CTRIA3      58      1      31      40      35
CTRIA3      59      1      40      39      35
CTRIA3      60      1      39      30      35
CTRIA3      61      1      31      32      36
CTRIA3      62      1      32      41      36
CTRIA3      63      1      41      40      36
CTRIA3      64      1      40      31      36
$
GRID         1      0     0.0    -2.0     0.0
GRID         2      0     0.0    -1.0     0.0
```

```
GRID            3       0     0.0     0.0     0.0
GRID            4       0     0.0     1.0     0.0
GRID            5       0     0.0     2.0     0.0
GRID            6       0    -0.5    -1.5     0.0
GRID            7       0    -0.5    -0.5     0.0
GRID            8       0    -0.5     0.5     0.0
GRID            9       0    -0.5     1.5     0.0
GRID           10       0    -1.0    -2.0     0.0
GRID           11       0    -1.0    -1.0     0.0
GRID           12       0    -1.0     0.0     0.0
GRID           13       0    -1.0     1.0     0.0
GRID           14       0    -1.0     2.0     0.0
GRID           15       0    -1.5    -1.5     0.0
GRID           16       0    -1.5    -0.5     0.0
GRID           17       0    -1.5     0.5     0.0
GRID           18       0    -1.5     1.5     0.0
GRID           19       0    -2.0    -2.0     0.0
GRID           20       0    -2.0    -1.0     0.0
GRID           21       0    -2.0     0.0     0.0
GRID           22       0    -2.0     1.0     0.0
GRID           23       0    -2.0     2.0     0.0
GRID           24       0    -2.5    -1.5     0.0
GRID           25       0    -2.5    -0.5     0.0
GRID           26       0    -2.5     0.5     0.0
GRID           27       0    -2.5     1.5     0.0
GRID           28       0    -3.0    -2.0     0.0
GRID           29       0    -3.0    -1.0     0.0
GRID           30       0    -3.0     0.0     0.0
GRID           31       0    -3.0     1.0     0.0
GRID           32       0    -3.0     2.0     0.0
GRID           33       0    -3.5    -1.5     0.0
GRID           34       0    -3.5    -0.5     0.0
GRID           35       0    -3.5     0.5     0.0
GRID           36       0    -3.5     1.5     0.0
GRID           37       0    -4.0    -2.0     0.0
GRID           38       0    -4.0    -1.0     0.0
GRID           39       0    -4.0     0.0     0.0
GRID           40       0    -4.0     1.0     0.0
GRID           41       0    -4.0     2.0     0.0
$
SPC             1       3  123456     0.0
SPC             1      12  123456     0.0
SPC             1      21  123456     0.0
SPC             1      30  123456     0.0
SPC             1      39  123456     0.0
MAT1*                   1          10.6E6                              .33+MA    1
*MA    1                                                0.              +MB    1
PSHELL*                 1               1          .0625               1+PA    1
*PA    1               1.               1       .8333333               0.
PARAM   AUTOSPC YES
PARAM      POST      -2
ENDDATA
```

BIBLIOGRAPHY

1. Bisplinghoff, Raymond L. and Holt Ashley. Principles of Aeroelasticity. New York: Dover Publications, Inc, 1975

2. Clough, Ray W. and Philip C. Johnson. "A Finite Element Approximation for the Analysis of Thin Shells," International Journal of Solids and Structures, 4: 43-60 (month,1968)

3. Cook, Robert D. Concepts and Applications of Finite Element Analysis(Second Edition). New York: John Wiley & Sons, 1981.

4. Dowell, Earl H. and others. A Modern Course in Aeroelasticity. Alphen aan den Rijn, The Netherlands: Sijthoff & Noordhoff International Publishers B.V., 1978.

5. Hearn, E. J. Mechanics of Materials (Second Edition). New York: Pergamon Press, 1985.

6. Karamcheti, Krishnamurty. Principles of Ideal-Fluid Aerodynamics. Malabar, Florida: Robert E. Krieger Publishing Company, Inc, 1980.

7. MacNeal, Richard H. ed. MSC/Nastran Technical Reference Manual (level 15.5). Los Angeles: MacNeal-Schwendler Corp., 1972

8. Mracek, Capt Curtis P. Unsteady Potential-Flow Solution Using Vortex Panels Coupled With Dynamics and Controls. PhD dissertation. Virginia Polytechnic Institute and State University, Blacksburg, VA, 1988. (AD-A197091).

9. Noble, Ben and James W. Daniel. Applied Linear Algebra (second edition). Englewood Cliffs, NJ: Prentice Hall, Inc., 1977.

10. Reymond, Michael A. MSC/Nastran Users Manual Volume I (version 66). Los Angeles: MacNeal-Scwendler Corp., 1988.

11. Rodden, William P. "Dihedral Effect of a Flexible Wing," The Journal of Aircraft 2:4. 368-373 Sept.-Oct. 1965

12. Roskam, Jan. Airplane Flight Dynamics and Automatic Flight Controls. Ottowa, KA: Roskam Aviation and Engineering Corp., 1982.

13. Saada, Adel S. Elasticity Theory and Applications. Malabar Florida: Robert E. Krieger Publishing Company, 1987

14. Schaeffer, Harry G. MSC/Nastran Primer: Static and Normal Mode Analysis. Mont Vernon, NH: Schaeffer Analysis, Inc, 1984.

15. Schneider, G. and H. Zimmerman. Static Aeroelastic Effects on High-Performance Aircraft. Report No. AGARD-R-725, Jan. 1986. (AD-A167595).

16. Triplet, William E. "Aeroelastic Tailoring in Fighter Aircraft Design". AIAA Papers 20th Structures, Structural Dynamics, and Materials Conference Part 1. 72-78, 1979.

17. Wilson, E. G. Static Aeroelasticity in the Design of Modern Fighters. Report No. AGARD-R-725, Jan. 1986. (AD-A167595).

18. Woodcock, J. (project engineer) Aeroelasticity in Stability and Control: Technical Report, March 1957. Contract AF33(616)-2424. J.B. Rea Company Inc. (AD-126-837).

Vita

Captain Raymond C. Maple

Cincinnati, Ohio. In 1981,

He then attended Cornell University on a four year AFROTC scholarship, earning the degree of Bachelor of Science in Mechanical Engineering in 1985. Upon graduation he received his commission in the USAF. He then served with the 3925th ICBM Facilities Engineering Squadron as a Minuteman Hardness and Survivability Engineer and Minuteman Systems Mechanical Engineer until entering the School of Engineering, Air Force Institute of Technology, in May 1988.

SECURITY CLASSIFICATION OF THIS PAGE

REPORT DOCUMENTATION PAGE

Form Approved
OMB No. 0704-0188

1a. REPORT SECURITY CLASSIFICATION UNCLASSIFIED	1b. RESTRICTIVE MARKINGS
2a. SECURITY CLASSIFICATION AUTHORITY	3. DISTRIBUTION/AVAILABILITY OF REPORT Approved for public release; distribution unlimited
2b. DECLASSIFICATION/DOWNGRADING SCHEDULE	
4. PERFORMING ORGANIZATION REPORT NUMBER(S) AFIT/ENY/GAE/89D-22	5. MONITORING ORGANIZATION REPORT NUMBER(S)
6a. NAME OF PERFORMING ORGANIZATION School of Engineering 6b. OFFICE SYMBOL (If applicable) AFIT/ENY	7a. NAME OF MONITORING ORGANIZATION
6c. ADDRESS (City, State, and ZIP Code) AIR FORCE INSTITUTE OF TECHNOLOGY Wright-Patterson AFB, Ohio 45433-6583	7b. ADDRESS (City, State, and ZIP Code)
8a. NAME OF FUNDING/SPONSORING ORGANIZATION 8b. OFFICE SYMBOL (If applicable)	9. PROCUREMENT INSTRUMENT IDENTIFICATION NUMBER
8c. ADDRESS (City, State, and ZIP Code)	10. SOURCE OF FUNDING NUMBERS PROGRAM ELEMENT NO. / PROJECT NO. / TASK NO. / WORK UNIT ACCESSION NO.

11. TITLE (Include Security Classification)
AN ITERATIVE SOLUTION TO AEROELASTIC EFFECTS IN POTENTIAL FLOW

12. PERSONAL AUTHOR(S)
Raymond C Maple, BS, Capt, USAF

13a. TYPE OF REPORT	13b. TIME COVERED	14. DATE OF REPORT (Year, Month, Day)	15. PAGE COUNT
MS Thesis	FROM _____ TO _____	1989 December	100

16. SUPPLEMENTARY NOTATION

17. COSATI CODES			18. SUBJECT TERMS (Continue on reverse if necessary and identify by block number)
FIELD	GROUP	SUB-GROUP	AEROELASTICITY FINITE ELEMENT ANALYSIS
20	04		
12	01		

19. ABSTRACT (Continue on reverse if necessary and identify by block number)

Thesis Advisor: Curtis P. Mracek
Capt, USAF

20. DISTRIBUTION/AVAILABILITY OF ABSTRACT ☐ UNCLASSIFIED/UNLIMITED ☐ SAME AS RPT. ☐ DTIC USERS	21. ABSTRACT SECURITY CLASSIFICATION UNCLASSIFIED
22a. NAME OF RESPONSIBLE INDIVIDUAL Curtis P. Mracek Capt, USAF	22b. TELEPHONE (Include Area Code) (513) 255-3517 22c. OFFICE SYMBOL AFIT/ENY

DD Form 1473, JUN 86 *Previous editions are obsolete.* SECURITY CLASSIFICATION OF THIS PAGE

The purpose of the study was to develop a method of incorporating static aeroelastic effects into a vortex paneling aerodynamic solution. The study had two basic objectives: (1) Devise a solution technique; (2) Implement the technique and analyze several test cases.

An iterative solution is developed which uses MSC/NASTRAN to perform structural analysis, and a three-dimensional vortex paneling method to perform aerodynamic analysis. The theory behind the method and details of the implementation are presented.

The method is tested for three bodies: a unit aspect ratio rectangular flat plate wing, a rectangular flat plate wing with aspect ratio 6, and a hollow sphere. Results of these tests are used to evaluate both the general performance of the implementation, and the performance for the specific tests. The results indicate that the iterative solution method is robust and could potentially be used for solving a variety of aeroelastic problems. Recommendations for further development, evaluation, and use are made.